Low Intensity IR Detection along with Photonic Synaptic device fabrication using 2D Reduced Graphene Oxide & Graphene Quantum Dots for enhancing Artificial Visual System.

A thesis submitted towards partial fulfilment of the requirements for the degree of

Master of Technology in Nanoscience and Technology

Submitted by :

ARIJIT ROY
Roll No. : M4NST24022

under the guidance of
Prof. (Dr.) Sourav Sarkar
School of Materials Science and Nanotechnology

Jadavpur University
Kolkata – 700032

Course Affiliated to:

Faculty of Interdisciplinary Studies, Law and Management
Jadavpur University
Kolkata, India
2024

M.Tech. (Nanoscience and Technology)
Course affiliated to :
Faculty of Interdisciplinary Studies,
Law and Management
Jadavpur University
Kolkata, India

CERTIFICATE OF RECOMMENDATION

This is in order to certify that the thesis entitled as " Low Intensity IR Detection along with Photonic-Synaptic device fabrication using 2D Reduced Graphene Oxide & Graphene Quantum Dots for enhancing Artificial Visual System." is a legitimate work done by Arijit Roy under our supervision and guidance for the purposes of fulfilling the requirement for the degree of Master of Technology in Nanoscience and Technology in the School of Materials Science and Nanotechnology from the academic session 2022-2024.

Thesis Advisor
Dr. Sourav Sarkar
School of Materials Science and
Nanotechnology
Jadavpur University
Kolkata - 700032

Director
School of Materials Science and
Nanotechnology
Jadavpur University
Kolkata - 700032

Dean
Faculty Council of Interdisciplinary Studies, Law and Management
Jadavpur University
Kolkata - 700032

M.Tech. (Nanoscience and Technology)
Course affiliated to :
Faculty of Interdisciplinary Studies,
Law and Management
Jadavpur University
Kolkata, India

CERTIFICATE OF APPROVAL

I hereby endorse the foregoing as an engineering study, conducted and presented in a manner satisfactory enough to justify it's acceptance as an engineering study, in order to obtain the degree for which it has been submitted. This approval does not endorse or approve any statement made, opinion expressed or conclusion drawn therein but merely approves the thesis for the purpose for which it has been submitted.

Committee of the final examination
for evaluation of the Thesis

_____
_____
_____
_____

**Only in the case thesis is approved.

DECLARATION OF ORIGINALITY AND COMPLIANCE OF ACADEMIC ETHICS

I hereby declare that this thesis contains literature survey and original research work by the undersigned candidate for the Master of technology (Nanoscience and Technology) programe during the academic year 2022-2024.

The information in this document has been gathered and presented according to the acdemic standards and ethical conduct.

I also declare that I have cited and referred to all materials and results that are not original to this work as required by these rules and conduct.

Name: ARIJIT ROY.
Roll No.: M4NST24022
Thesis Title : Low Intensity IR Detection along with Photonic-Synaptic device fabrication using 2D Reduced Graphene Oxide & Graphene Quantum Dots for enhancing Artificial Visual System.

Date : **SIGNATURE**

ACKNOWLEDGEMENT

I am grateful to **Dr. Sourav Sarkar** my adviser, for his consistent encouragement, passion, and wide knowledge throughout my Master's studies and research. He was there for me every step of the way as I worked on my thesis. Your informative comments inspired my entire research project, and I am grateful. In addition, I'd want to express my gratitude to **Prof. Kalyan Kumar Chattopadhyay** and the Thin Film and Nano Science Lab, as well as the Nanoscience and Nanotechnology Lab, for establishing a friendly work environment for me.

Mr. Manas Thakur, my mentor, deserves my gratitude for his direction and assistance with all of my project-related issues, as well as for cooperating with me to make it what it is now.

I gratefully thank **Prof Kalayan Kumar Chattopadhaya**, **Dr. Sourav Sarkar**, **Dr. Mahua Ghosh**, and **Dr. Chandan Kumar Ghosh** for their assistance, support, recommendations, and guidance. They offered a helpful and constructive learning environment, and their excitement inspired me to pursue the research topic with zeal.

Sk Najes Riaz, Ankita Chandra, Nabanita Sen, Ratna Sarkar, Suvankar Poddar and Suvra Pal, my seniors, deserve my heartfelt gratitude for making my project such a memorable experience. I truly thank Soumili Kar, Koustav Samaddar, Arnab Kumar das and my classmates for their assistance and support throughout this course. I could not have completed my project without their assistance. In light of their tremendous aid, my words of gratitude are insufficient.

Finally, I want to express my heartfelt gratitude to my parents and all of my supporters for their love and support.

Abstract

Information sensing, processing and memory operation are the building blocks Artificial Visual System. Photonic Synapse is a promising component that can enhance the visual processing efficiency owing to the fast responsivity, low power consumption and large bandwidth. Herein, a Photo-synapse has been constructed having heterostructure configuration between Reduced Graphene Oxide (rGO) and Graphene Quantum Dot (GQD) which have been synthesized with a simple Hydrothermal method. By the high interfacial effect of high photosensitive characteristic of GQD and large surface area, enhanced semiconducting bandgap and high charge carrier mobility performance of rGO 2D layer shows fundamental synaptic behaviours like Excitory Post Synaptic Current (EPSC), Pair Pulse Facilitation (PPF), plasticity i.e. transition from short term memory (STM) to long term memory (LTM) etc. Following the completion of all required characterizations of materials, such as XRD, UV-Vis, and PL, we began optimizing our device with the appropriate light intensity. The final optimized version of our device is having an area of channel region 2×4 mm^2 with a 2 layers of rGO and 1 layer of GQD. One of the key point of our device, it is showing good response in low intensity Infra-Red radiation which totally neutralize the effect of thermal noise which is an essential issue while working with IR. At last the different synaptic performance like it's EPSC, PPF, Plasticity etc. of the device has been successfully stimulated. Not only that our device is showing a very good non-volatile memory nature and stability at STM.

Contents

1 Introduction **10**

1.1 Introduction to Nanotechnology : 10
1.2 Two Dimensional Materials : 11
1.2.1 Applications of Two Dimensional Materials : 13
1.3 Quantum Dots : 14
1.3.1 Applications of Quantum Dots : 15
1.4 Reduced Graphene Oxide : 16
1.5 Graphene Quantum Dots : 17
1.6 Introduction to Neuromorphic Computing : 19

2 Instrumentation : **24**

2.1 Morphological Characterizations : 24
2.1.1 Scanning Electron Microscope : 24
2.1.2 Transmission Electron Microscope : 27
2.2 Phase or Crystallographic characterization : 29
2.2.1 X-Ray Diffraction (XRD): 29
2.3 Spectroscopic Characterization : 33
2.3.1 UV-VIS near Infrared Spectroscopy: 33
2.3.2 Fourier Transform Infra-Red Spectroscopy : 34
2.4 I-V Characterization : 37

3 Literature Review: **39**

3.1 Synthesis Technique : 39
3.1.1 GO synthesis using Staudenmaier's (ST) method: . . . 40
3.1.2 Hydrothermal Process : 40
3.2 Review of Photonic Synapses : 42

3.2.1 Perovskite/Organic semiconductor based Photo- nic Synapses : 42
3.2.2 Ferroelectric van dar waals heterostruture based Photonic Synapses : 42

4 Synthesis of Materials: 45
4.1 Synthesis of GO using modified Hummer's method : 45
4.2 Synthesis of rGO and GQD using Hydrothermal Method : . . 47

5 Characterization of Materials: 49
5.1 Morphological Characterization & Analysis : 49
5.1.1 Field Emission Scanning Electron Microscopy (FESEM) of rGO : 49
5.1.2 High-resolution transmission electron microscopy (HRTEM) of GQD : 50
5.2 Crystallographic Characterization & Analysis : 51
5.2.1 X-Ray Diffraction of rGO & GQD : 51
5.3 Spectroscopic Characterization & Analysis : 52
5.3.1 UV-Vis Spectroscopy of rGO & GQD: 52
5.3.2 Fourier Transform Infra-Red Spectroscopy (FTIR) of rGO : 55
5.3.3 Photo-luminescence (PL) of GQD : 56

6 Device Fabrication: 60

7 Results and Discussion: 64
7.1 Analysis of Device with Different Light Illumination : 64
7.2 Device Performance with a specific Incident Light : 67
7.3 Optimization of Device : 69
7.4 Selection of proper Intensity of Light : 71
7.5 Evaluating the performance of Memory function : 71
7.5.1 Excitory Post Synaptic Current (EPSC)Variation: . . 71
7.5.2 Pair Pulse Facilitation (PPF) Index : 74
7.5.3 Plasticity Performance (Transition from STM to LTM) : 76

8 Conclusion and Future Work : 80

List of Figures

1.1 **Structure of Graphene (Left) and Hexagonal -Boron Nitride (Right).** 12
1.2 **Geometric Structure of Molybdenum disulphide (MoS_2).** 12
1.3 **Crystal Structure of Phosphorene.** 13
1.4 **Confinement of Quantum Particle in Quantum Dot.** . . 15
1.5 **Reduction of Graphene to GO and then rGO.** 17
1.6 **Optimizied Structure of GQD** 18
1.7 **Comparison of the von Neumann architecture with the neuromorphic architecture.** 21

2.1 **FESEM (Hitachi S-4800) set up** 27
2.2 **FESEM (FEI Tecnai TEM.)** 29
2.3 **FESEM (Brag's Law of diffraction** 30
2.4 **Production of X-Rays.** 31
2.5 **X-Ray Diffraction (Bruker D8 advance.)** 32
2.6 **Production of X-Rays.** 34
2.7 **Process of generating an FTIR spectra.** 35
2.8 **Internal components of FTIR instrument.** 36
2.9 **Two probe device used in the project.** 37

4.1 **Schmatic of Synthesis Procedure of GO,rGO and GQD.** 46

5.1 **FESEM Image of rGO.** 50
5.2 **HRTEM Image of GQD.** 51
5.3 **XRD Plot of GQD.** 52
5.4 **UV-Vis Absorption Spectra of rGo** 53
5.5 **UV-Vis Absorption Spectra of GQD.** 54
5.6 **Tauc plot and band calculation of rGO.** 54
5.7 **Tauc plot and band calculation of GQD.** 55

5.8 **FTIR Plot of rGO.** 56
5.9 **PL plot of GQD.** 57

6.1 **Schematic of Device Fabrication.** 61
6.2 **Final Device.** 61
6.3 **Optimization of devices (a) Length-wise and (b) Breadth-wise.** 62

7.1 **DRS Plot of Devices with different layer numbers.** . . 65
7.2 **I-V characteristic and LogI-V Plot of different layered devices.** 66
7.3 **I-V characteristic and LogI-V Plot under different light illumination.** 68
7.4 **(a) Length-wise and (b) Breadth-wise Optimization of device.** 70
7.5 **(Left to Right) Variation of Photo-current with different Intensity of Light, Resonsivity with different light intensity.** 71
7.6 **(Left to Right) EPSC at operating voltage -2 V and -1 V .** 72
7.7 **EPSC evoked by different light pulse width.** 73
7.8 **Variation of EPSC with pulse width under a light pulse.** 74
7.9 **EPSC triggered with two successive pulses** 75
7.10 **Variation of PPF index with pulse interval between two light pulses.** 76
7.11 **Left to Right) Transition from STP to LTP by increasing pulse width and pulse number.** 77
7.12 **Relative Intensity changes of EPSC with light pulse width.** 78

Chapter 1

Introduction

1.1 Introduction to Nanotechnology :

The Greek word meaning dwarf is the source of the prefix "nano." A nanometer (nm) is the same as ten-nine meters, or one-billionth of a meter. A human hair is roughly 80,000 nanometers wide, and a red blood cell with a width of about 7000 nm. Atoms are less than a nanometer, but many molecules can range in size from a nanometer to several proteins. The manipulation of materials at the molecular or atomic level is known as nanoscience and technology. in order to create new, improved, and remarkable materials and devices attributes. Nanotechnology is not a brand-new field, though. Instead, it is the combining of several scientific fields (chemistry, biology, physics, engineering, and medicine) and the combination of skills to customize materials at the nanoscale, roughly between 1 and 100 nanometers.

Theoretical framework of nanotechnologies was initially presented by physicist during his talk, "There's plenty of room at the bottom," Richard Feynman (Feynman 1959). Feynman investigated the potential for material manipulation at the size of individual atoms and molecules, envisioning the entire Britannica printed on the head of a pin and anticipating the growing capacity to study and manipulate matter at the nanoscale.

It was not until 1974 that the phrase "nanotechnology" was adopted by Norio Taniguchi, a researcher at the It was introduced by the University of Tokyo in Japan to describe the capacity to precisely modify materials at the at the nanoscale level. At the time, the main factor pushing miniaturization was the electronics sector, which sought to provide instruments for producing

smaller (and hence faster and more intricate) silicon-chip electrical devices. In fact, IBM in the USA uses a method called electron beam lithography was used to create nanostructures and devices as small as 40–70nm in the early 1970s.

1.2 Two Dimensional Materials :

When the size and the dimension of a material continuously reduced from macroscopic to the nanometer scale the properties of the material begin to changes to a certain level. When the size becomes below 100 nm the common features totally being abolished and new changes occur drastically. If one dimension rerduced to nano scale and other two remain large, then we obtain a structure of Two Dimensional Material (2D Material)or quantum well. If two of the dimension reduced to nanometer scale it becomes one dimensional (1D) material or quantum wire; if all of the dimension reduced to nanometer range, then the structure of materials obtained as zero dimensional (0D) material od quantum dot.

This section is only dedicated to 2 D materials, which grabs interesting research attention from last few years. 2D Nanomaterials with certain geometries exhibit unique shape-dependent characteristics and subsequent utilization as building blocks for the key components of nanodevices. The strong features of 2D materials like large surface to volumn ratio, induction of defects in the surface, it's compatibility with other dimensional materials makes it very promising material for future development of the devices.

1. **Graphene and Hexagonal Boron-Nitride :**

   Graphene is a covalently-bonded hexagonal lattice of carbon atoms just one atom thick (about 0.14 nm). It is a semimetal (its conduction and valence bands both touch). Graphene's unique band structure means that electrons move through it at extremely high speeds (about 1/300 the speed of light), giving it fascinating properties - such as unparalleled thermal conductivity. Optically transparent, graphene absorbs only 2 percent of incident visible light and has the highest tensile strength of any material. A single monolayer of graphene, just 0.3 nm thick, would be able to support the weight of a football.

   Hexagonal boron nitride (h-BN) is an isomorph of graphene (has the same crystallographic appearance), but has boron and nitrogen atoms

instead of carbon. In contrast to graphene, it is a wide-bandgap insulator.

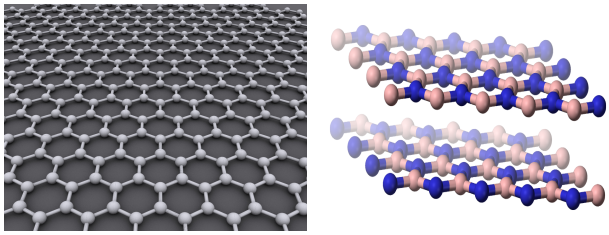


Figure 1.1: **Structure of Graphene (Left) and Hexagonal -Boron Nitride (Right).**

2. **Transition Metal Dichalcogenides (TMDCs) :**

   Transition Metal Dichalcogenides have the chemical formula MX_2, where M stands for transistion metals like molybdenum (Mo) or tungsten (W) and X belongs chalcogens such as sulfur (S), selenium (Se) or Tellurium (Te) etc. Bulk TMDCs are three layers thick where the metal is sandwiched between two layers of chalchogens. These materials posses different crystallographic geometry structure, out of them the common one's are 2H-phase with trigonal symmetry possessing semiconductor nature like MoS_2, WSe_2, $MoSe_2$ etc and metallic 1T phase such as WTe_2.

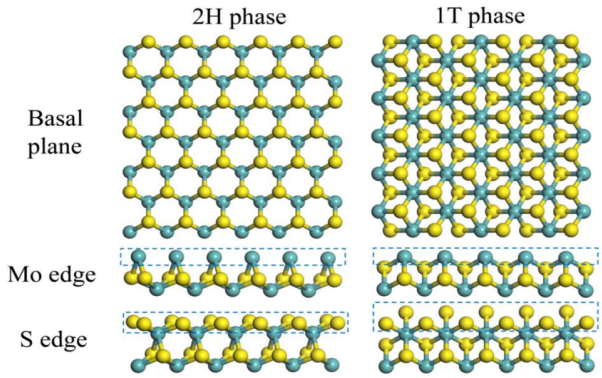


Figure 1.2: **Geometric Structure of Molybdenum disulphide (MoS_2).**

3. **Phosphorene :**

   Phosphorene is a single layer of black phosphorus – a layered, stable allotrope of elemental phosphorus. t is a direct bandgap semiconductor with a puckered honeycomb structure. The band gap value can be tuned to visible light spectra by incorporating multiple layers. It has good charge mobility, therefore making it suitable for optoelectronic devices and transistors.

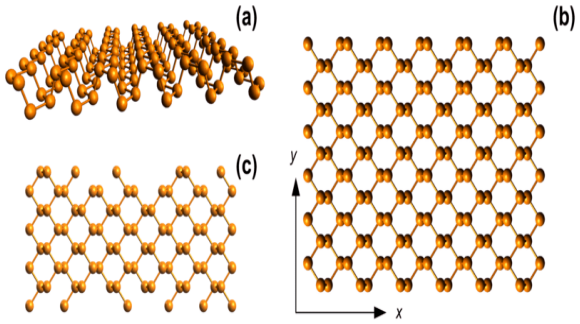


Figure 1.3: **Crystal Structure of Phosphorene.**

1.2.1 Applications of Two Dimensional Materials :

1. **Transistors and Sensors :** Field Effect Transistors (FETs) are fabricated with variety of semiconducting 2D materials because of it's enhanced mobility performance and it's moderate band gap makes it a potential component for this application. Hexagonal boron nitride is often used as the gate dielectric. The semiconducting materials belonging the Graphene family are used as active channel of transistors because of it's engineering edge states, chemical doping, and less scattering of majority carriers. Using TMDCs in a FET based sensors are being used very actively in this decade, those have been used to detect different range of chemicals like triethylamine , nitric oxide, ammonia, and nitrogen dioxide by measuring changes in conductance or resistance or capacitance when exposed to these chemicals.

2. **Photdetectors :** Many TMDCs such as MoS_2, WSe_2, $MoSe_2$ etc. are being used as the photo-detection application. The moderate en-

hanced bandgap nature of these materials enble them it's upgraded performance of optical detection behaviour. The composites of this materials with other candidates enhance it's optical property and and help to detect a wide range of spectral light within a single device. At last it's fast resposivity and high detectivity makes these materials a potential candidate for poeto-detction application.

3. **Battery Electrodes :** Electrodes for ion batteries and supercapacitors require electrically conductive materials with a high surface area to store high densities of ions. Graphene has received some attention as a possible successor to graphite electrodes due to its higher surface-to-mass ratio, higher conductivity, greater mechanical strength, and flexibility.

1.3 Quantum Dots :

Quantum dots are semiconductor nano crystals with a dimension in nanometer scale which provides quantum confinement behaviour towards any quantum particle. Their size effects the optical as well as electrical property the material to a certain level. When QDs are irradiated with any light illumination , the majority carrier in the QD can be excited from the valence band to the conduction band or vice versa, and upon its relaxation it emits radiation in a particular spectral region. QDs have narrow fluorescence emission bands, but broad absorption bands, therefore, they are prominent optical transducers. QD emission wavelengths can be easily tuned by varying the size, shape, or composition of the QD. Hence, QDs are perfect for multiplex detection of various substances

Based on their chemical composition and architecture QDs can be categorized into various types such as core type, core-shell, and alloyed quantum dots. These QDs have the ability to emit a wide spectrum of wavelength (light) under UV radiations. When QDs are irradiated considerable number of electrons have energized and ejected from their atoms facilitating the formation of a conduction band where electrons are allowed to move throughout that material. If these electrons back to the valence band they emit light, and the wavelength of light depends on the energy gap between the valence band and conduction band.

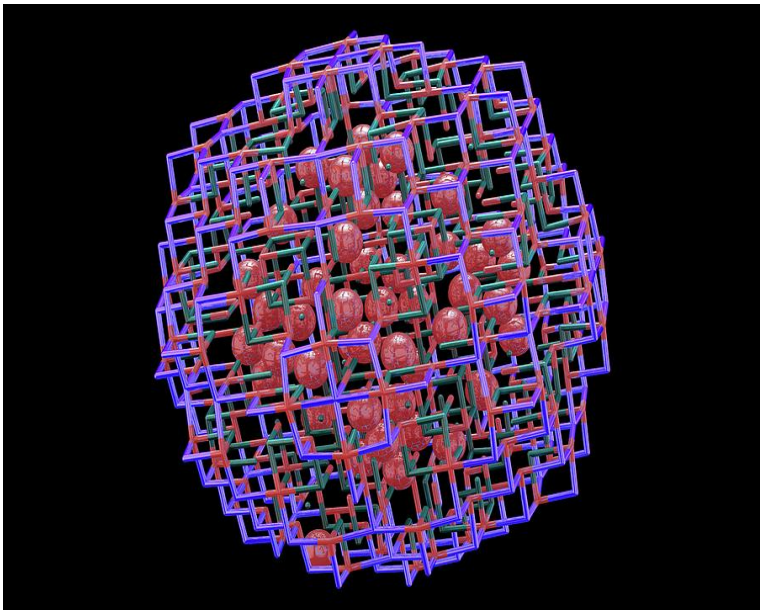


Figure 1.4: **Confinement of Quantum Particle in Quantum Dot.**

1.3.1 Applications of Quantum Dots :

1. **Display Devices :** QDs have potential in construction of Light - emitting tools with a very high efficiency of emitting performance. QD-based LEDs showcase notably improved and precise color representation. Compared to conventional displays, modern displays offer higher contrast ratios, and brightness, consume less power, have higher resolutions, highly immersive high-dynamic range (HDR) experience. QDs' narrow emission spectra and wide excitation profiles make it more convenient to convert light into any color within the visible spectrum.

2. **Biomedical Applications :** High luminescence, narrow emission, low toxicity properties make QDs as avery good promising candidate for bio imaging, bio-sensing applications. For instance, fibrous phosphorus QDs were demonstrated as fluorescent labels for human adenocarcinoma bioimaging. Qds also have a number of attractive features in drug delivery systems including including their ease of fabrication, capability of conjugation to a wide variety of drugs.

Out of above mentioned materials, Reduced Graphene Oxide (rGO) and

Graphene Quantum Dot (GQD) are the potential candidate for our work investigation. Next section is totally devoted for the analysis of these materials;

1.4 Reduced Graphene Oxide :

Reduced Graphene Oxide (rGO) is one of the famous 2D material because of it's different, unique properties and efficient applications in daily life. It's high conductivity, large surface area, high chemical stability and it's tremendous carrier mobility performance nature grabs much attention of researchers especially in the field of nanotechnology. This superior characteristics of rGO makes it a potential material in different aspect of devices like electrochemical sensors, energy storage device, memory devices etc.

Graphite restacks easily, making the chemical production of large-scale single-layer graphene sheets from raw graphite extremely difficult. To neutralize this issue firstly, Graphite sheets are being chemically oxidized for the making of single layerd Graphene Oxide (GO) which is then converted into reduced Graphene Oxide which has exact similar properties with the graphene because of it's large surface area and porosity nature. To date, different reducing agents have been utilized like hydrazine, hydroxylamine, urea, dimethyl ketoxime, pyrrole, ammonia, and pyrrolidine to convert rGO from GO. Several oxygen-containing groups have been added, including ascorbic acid, gallic acid, hydroquinone, and metal particles like Fe powder and Zn/HCL. The functional group which contains the oxygen and nitrogen mentioned earlier have been chosen above other chemicals for reduction purposes because these functionalities on the carbon moiety can start the production of sp^3 carbon and defect density which enable different electrochemical features of the material. By adjusting the reaction's time and temperature the optimum rGo can be produced and also can be used for different sensing purposes. Not only these, the composite of rGO with different materials makes the device a very promising interms of photo sensors.

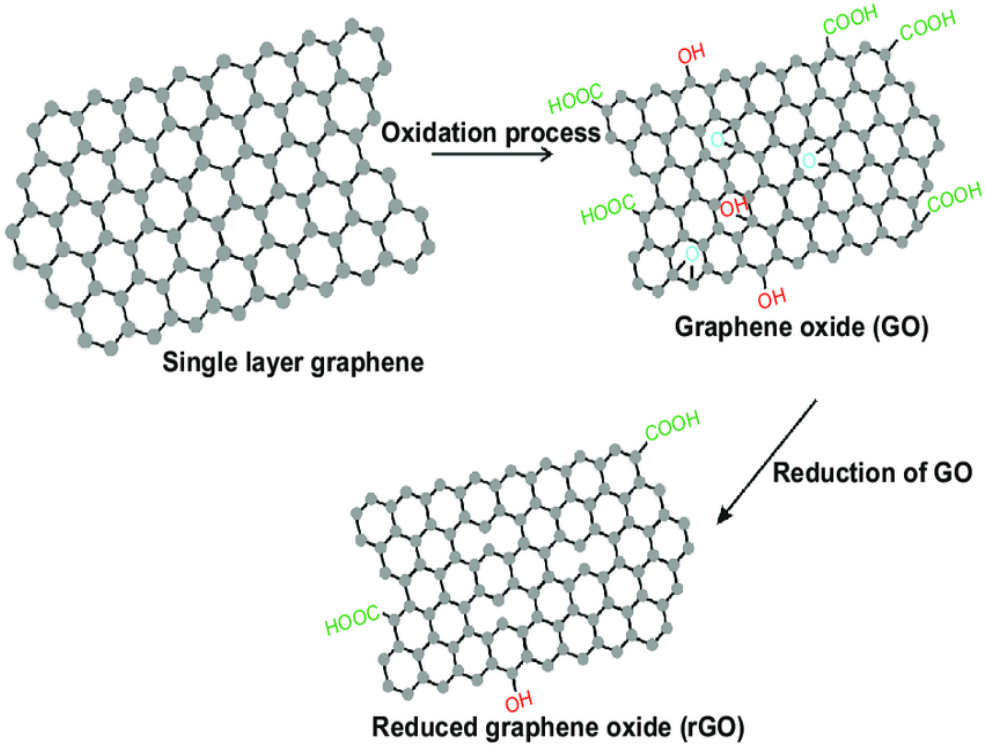


Figure 1.5: **Reduction of Graphene to GO and then rGO.**

1.5 Graphene Quantum Dots :

Graphene Quantum Dots (GQD) are carbon based particles and a family member of graphene family. GQDs are tiny segments of graphene whose electron mobility confine in all three dimensions also it posses infinite exciton Bohr diameter. This type of materials have less than 10 nm of size. Due to the large surface to mas ratio, easily dispersive nature in water makes the GQDs very stable physically as well as chemically. Size tunability effets makes the GQDs a very emergent choice of material in the field of photodectors, biosensors etc. The fluorescence emission of GQD varies a wide spectral range including UV, Visible, IR etc. still the fluorescence emission property is a debatable thing to discuss as it has quantum confinement, defect states and functional groups that might depend on the pH, when GQDs are dispersed in water. In general, if the no. of graphene layer increases the band gap of GQD will going to reduce.

This versatile characteristics of GQD makes it very sophisticated material in aspects of science. Because of it's unique optical, electrical and photoelectric properties it can be used in bioimaging, biosensors, temperature sensors, dru delivry, photodetectors , solar cell etc.

At present there are different techniques for the preparation of GQDs. All of them are mainly classified into two divisions Bottom Up and Top Down methods. Top Down method approaches different procedures to cut bulk graphite materials like graphene, carbon nanotubes, coal, carbon blavk etc. This techniques includes chemical synthesis, electro beam lithography, Graphene Oxide reduction, microwave synthesis, hydrothermal method and so on. But in top down method intense purification of materials are an essential need. Whereas, bottom up methods assemble GQDs from small organic molecules such as citric acid and glucose. These GQDs have better biocompatibility.

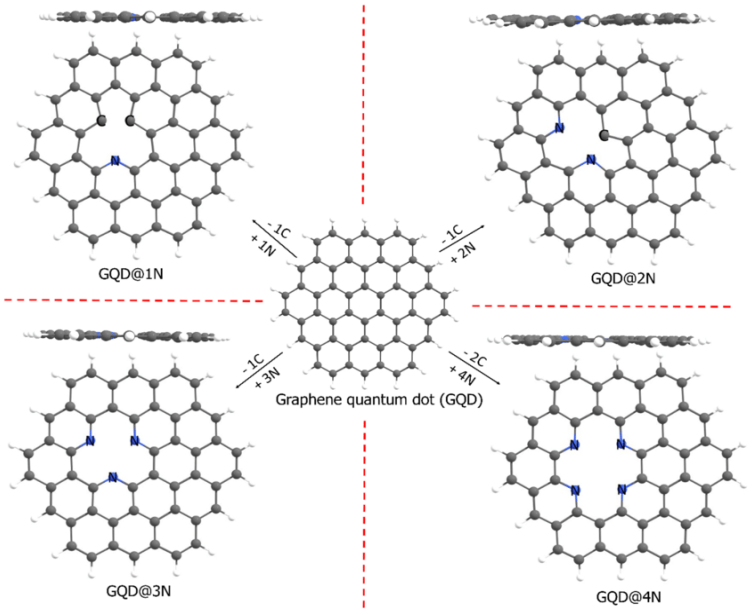


Figure 1.6: **Optimizied Structure of GQD**

1.6 Introduction to Neuromorphic Computing :

The computer community is increasingly looking at new technologies to provide ongoing performance advances as Dennard scaling and Moore's law draw to an end. One such emerging computing technology is the neuromorphic computer. Carver Mead first used the term "neuromorphic" in the late 1980s to describe mixed analogue-digital brain-inspired computing implementations. However, as the field has developed and large-scale funding opportunities for brain-inspired computing systems have emerged, such as the DARPA Synapse project and the Human Brain Project of the European Union, the term has expanded to include a wider range of hardware implementations.

Neuromorphic computers are non-von Neumann computers made of synapses and neurons whose structure and functions are modeled after brains. Von Neumann computers consist of distinct central processing units (CPUs) and memory units, the latter of which stores instructions and data. On the other hand, the neurons and synapses control memory and processing in a neuromorphic computer. Unlike von Neumann computers, which use explicit instructions to construct programs, neuromorphic computers use the structure and properties of the neural network to define programs. Additionally, neuromorphic computers take spikes as input, where the corresponding time at which they occur, their amplitude, and their shape are represented. In contrast, von Neumann computers encode information as numerical values represented by binary values.

Given the aforementioned contrasting characteristics between the two architectures (Fig. 1.7)[5,6], neuromorphic computers present some fundamental operational differences;

- **Extremely parallel operation:** Compared to parallelized von Neumann systems, the computations carried out by neurons and synapses in neuromorphic computers are comparatively easy. This is because all of the neurons and synapses have the potential to operate concurrently.

- **Collocated processing and memory:** Neuromorphic technology does not support the idea of processing and memory being separate entities. In many implementations, both neurons and synapses do processing and store information, despite the fact that neurons are some-

times thought of as processing units and synapses as memory. The von Neumann bottleneck relating to the processor/memory separation, which slows down the maximum throughput that may be reached, is lessened when processing and memory are colocated. Furthermore, as in traditional computing systems, this collocation aids in avoiding data accesses from main memory, which use a significant amount of energy in comparison to compute energy.

- **Inherent scalability:** neuromorphic computers are meant to be inherently scalable as adding additional neuromorphic chips entails increasing the number of neurons and synapses that can be realized. It is possible to take multiple physical neuromorphic chips and treat them as a single large neuromorphic implemen-tation to run larger and larger networks. This has been success-fully accomplished across a variety of large-scale neuromorphic hardware systems.

- **Event-driven computation:** To achieve incredibly efficient processing, neuromorphic computers make use of temporally sparse activity and event-driven computation, which involves computing only when data are available. Only when there are spikes to process do neurons and synapses function; normally, spikes are somewhat rare during network operation.

- **Stochasticity:** neuromorphic computers can include a notion of randomness, such as in the firing of neurons, to allow for noise.

The exceptionally low power consumption of neuromorphic computers they may frequently function on orders of magnitude less power than conventional computing systems is one of their most alluring computational capabilities. Because they operate in enormous parallel and are event-driven, only a tiny percentage of the system is usually active at any given moment, with the remainder being idle. This results in reduced power consumption. Energy efficiency alone is a strong argument for looking into the use of neuromorphic computers because of the rising cost of computing power and the growing number of applications where energy is limited (such as edge computing applications). Furthermore, neuromorphic computers are an ideal foundation for many of today's innovations since they naturally implement neural network-style computation.

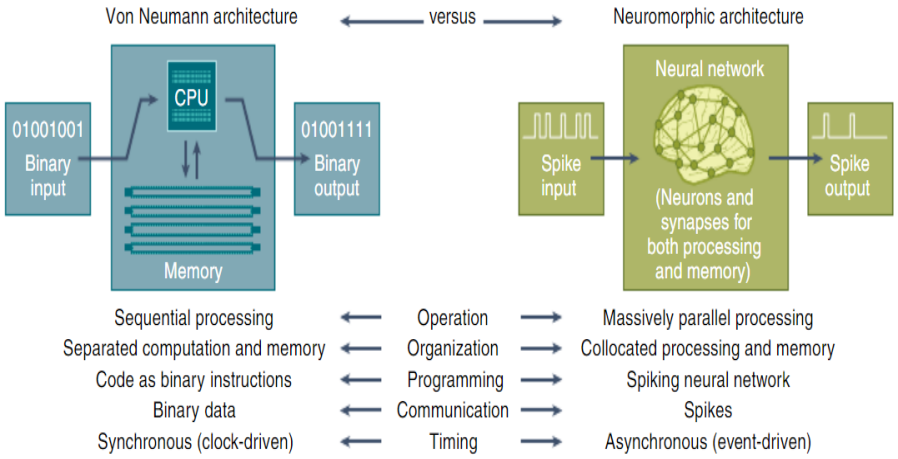


Figure 1.7: **Comparison of the von Neumann architecture with the neuromorphic architecture.**

Though it's unclear if they're the only aspects of biological brains that matter for computation, each of these features of neuromorphic computers has been prioritized in the implementation of these devices, which are all inspired by features found in the brain. For instance, a number of different brain components may be helpful for computation even though neurons and synapses have been selected as the main computational units of neuromorphic computers. Furthermore, while neurons and synapses have proven to be a useful abstraction level for neuromorphic computers, it is still debatable if this is the best level of abstraction.

In contrast to certain forthcoming computing technologies, numerous physical embodiments of neuromorphic hardware are presently being development or are accessible for utilization by the scientific community. Numerous extensive neuromorphic computers have been created using diverse methods and objectives. To enable neuroscience simulations at scale, SpiNNaker and BrainScaleS were developed with funding from the European Union's Human Brain Project. The online-learning digital spiking neuromorphic (ODIN), an improved digital neuromorphic processor, has also been proposed21; it permits the use of slightly more complicated neuron models. The Tianjic chip, which supports both classic artificial neural networks and neuromorphic spiking neural networks for various problem categories, is one of the neuromorphic platforms aimed at more general computations for broader kinds of applica-

tions. Neuromorphic systems have piqued the interest of both industry and academia. Examples of business projects include IBM's TrueNorth and Intel's Loihi, while academic efforts include DYNAPs, Neurogrid, IFAT, and BrainScales-. Neuromorphic hardware, like BrainScales-2, has proven useful in optimizing learning-to-learn scenarios—that is, in defining how learning happens—for spiking neural networks. These optimizations are carried out at much faster time scales than those of biological processes.

While a great deal of work is being done in the neuromorphic community to develop new materials for neuromorphic implementations, such as phase-change, ferroelectric, non-filamentary, topological insulators, or channel-doped biomembranes, all of the previously mentioned large-scale neuromorphic computers are silicon-based and implemented using conventional complementary metal oxide semiconductor technology. Although optoelectronic devices and memristors are two other common approaches in the literature for implementing neuromorphic computers, memristors are still considered the fundamental technology for resistive memory, which combines computation and memory. Each device and material used to implement neuromorphic computers has unique operating characteristics, such as how fast they operate, their energy consumption and the level of resemblance to biology. The diversity of devices and materials used to implement neuromorphic hardware today offers the opportunity to customize the properties required for a given application.

In order to fully utilize neuromorphic computers in the future, take advantage of all of their special computational qualities, and influence hardware design, neuromorphic algorithms and applications must be linked to neuromorphic computers. Currently, the majority of research in the field of neuromorphic computing focuses on the aforementioned hardware systems, devices, and materials. From this vantage point, we offer a synopsis of the most advanced neuromorphic algorithms and applications available today as well as an outlook on the potential uses of neuromorphic computing in computer science and computational science going forward. It is important to note that several distinct kinds of technologies have been referred to by the phrase "neuromorphic computing." As noted previously, the original definition only encompassed mixed ana-logue-digital implementations. In this work, we consider all types of hardware implementations (digital, mixed analogue-digital, analogue) as neuromorphic, but we restrict our attention to spiking neuromorphic computers, that is, those that implement spiking neural networks.

Bibliography

[1] S. Priya, D.J. Inman, Energy Harvesting Technologies, 2009, pp. 1e517, https:// doi.org/10.1007/978-0-387-76464-1.

[2] Brubaker DG, Fuller ML (1945) J Appl Phys 16:128

[3] D. E. Aspnes, "Optical properties of thin films,"Thin Solid Films, vol. 89, no. 3, pp. 249–262, 1982.

[4] G. Sberveglieri, "Recent developments in semiconducting thin film gas sensors," Sensors and Actuators B, vol. 23, no. 2-3, pp. 103–109, 1995.

[5] "Physics for neuromorphic computing" Danijela Marković, Alice Mizrahi, Damien Querlioz and Julie Grollier; Nature Reviews Physics volume 2; https://doi.org/10.1038/s42254-021-00358-7

[6] "Opportunities for neuromorphic computing algorithms and applications" Catherine D. Schuman, Shruti R. Kulkarni, Maryam Parsa, J. Parker Mitchell, Prasanna Date and Bill Kay ; Nature Computational Science 2; https://doi.org/10.1038/s43588-022-00223-2

[7] Mead, C. Neuromorphic electronic systems. Proc. IEEE 78, 1629–1636 (1990).

[8] Davies, M. et al. Loihi: a neuromorphic manycore processor with on-chip learning. IEEE Micro 38, 82–99 (2018).

Chapter 2

Instrumentation :

There are several different methods to characterize the sample to determine its phase, morphology, band gap, lattice vibration, crystallite size, interplanar distance, crystal plane etc. Here, in this work also these methods and machineries are being used to determine various properties of the prepared samples.

2.1 Morphological Characterizations :

Morphological characterization defines as the technique or method to get information about the morphology of the sample in micro and nano level. In nanotechnology, ordinary optical microscope can not be used due to their limited focus range which is not able to get the information in nano level. Hence, the need of electron microscopes has been emerged and resulting two types of very important electron microscope, i.e., **Scanning Electron Microscope (SEM)** and **Transmission Electron Microscope (TEM)**.

2.1.1 Scanning Electron Microscope :

One of the most adaptable tools for inspecting and deciphering the morphology of microstructures is the scanning electron microscope (SEM). The surface of the object is routinely scanned by a focused electron beam in a scanning electron microscope (SEM), yielding a significant number of signals. An image is produced from these electron impulses and displayed on a

cathode ray tube (CRT). There are two techniques to produce the electron beam:

a) Thermionic emission; b) Field emission.

Thermal energy is used to regulate the source's electron emission to produce thermionic emission. In modern electron microscopes, field emission electron guns (FEG) are a great replacement for thermionic electron guns. Very minute topographic characteristics on the surface of whole or fragmented objects can be observed with a FESEM. Researchers in the fields of biology, chemistry, and physics utilise this technique to examine structures as small as 1 nanometer, or billionths of a millimetre. Organelles and DNA material in cells, synthetic polymers, and microchip coatings can all be studied with the FESEM.

Sample Preparation for FESEM :

The specimens that can be analysed must be compatible with high vacuum (10-5 mbar), as the SEM is operated under high vacuum. This suggests that liquids and objects made of volatile substances, like water, cannot be directly studied. To prevent contaminating the SEM specimen chamber, fine powder samples must also be firmly connected to a specimen holder substrate. A thin conductive layer must be sprayed or evaporated onto non-conductive materials before they are attached to a conductive specimen container. Common coating materials include carbon, Au, Pt, Pd, and their alloys.

Components for FESEM :

1. **Electron Guns :**Modern FESEM systems require a constant electron beam from the electron cannon that has a high current, a small spot size, configurable energy, and minimal energy dispersion. A variety of electron guns are used in a FESEM system, and the quality of the electron beam produced by each differs greatly. The tungsten "hairpin" or lanthanum hexaboride (LaB6) cathodes used in the first FESEM systems have since been replaced by field emission sources, which provide more current and less energy dispersion. The longevity of the emitter is a crucial consideration when selecting electron sources.

2. **Electron Lenses :** Electron beams can be concentrated by electrostatic or magnetic fields. The FESEM system, however, solely employs

a magnetic field since an electron beam governed by one has less aberration. Electromagnets can be used to alter the electrons' routes.

3. **Condenser Lenses :** The electron beam will diverge after passing through an anode plate from the emission source. The electron beam is brought together and collimated by the condenser lens into a nearly parallel stream. Two rotationally symmetric iron pole pieces make form a magnetic lens, and a copper winding generates the magnetic field. The centre of each pole piece has a hole through which the electron beam can travel. Through a lens-gap between the two pole components, the magnetic field shapes (focuses) the electron beam. Condenser lens current can be changed to change the focus point's location.

4. **Scan Coils:** The scan coils cause the electron beam to be zigzagged as it passes over the object. The development of the image on the display and the scan movement are coordinated. The scan velocity controls both the screen's refresh rate and the amount of noise in the image. In scan coils, upper and lower coils are frequently utilized to avoid the formation of a circular shadow at low magnification.

5. **Objective Lenses :** The electron beam will diverge below the condenser aperture. The electron beam is de- magnified further and focused into a probe point on the specimen surface using objective lenses. The diameter of the electron beam on the specimen surface (spot size), which affects image resolution, decreases as aperture size and fundamentals of Scanning Electron Microscopy increase.

6. **Stigmator Coil :** The stigmator coils are used to rectify inconsistencies in the beam's xand y deflection, resulting in a perfectly round beam. When the beam is ellipsoidal rather than circular, the picture seems fuzzy andstretched.

7. **Objective Chamber :** The object is coated with a conductive coating before being set on a particular holder. The object is anchored on a moveable stage and introduced into the high vacuum section of the microscope through an exchange chamber. The secondary electron emission detector (scintillator) is placed behind the object holder in the chamber.

8. **Image Information :** Complex interactions take place when an electron beam impinges on a specimen surface in a FESEM and stimulates various signals for FESEM inspection. It is possible to collect and display secondary electrons, back scattered electrons (BSEs), transmitted electrons, and specimen current on a monitor. To determine the specimen's composition, the excited x-ray or Auger electrons are analysed. This part will cover the interactions of the electron beam with the specimen surface as well as the idea behind making pictures out of different signals.



Figure 2.1: **FESEM (Hitachi S-4800) set up**

2.1.2 Transmission Electron Microscope :

A beam of electrons is transmitted through a material to create a picture in the microscopy technique known as transmission electron microscopy (TEM).

Most frequently, the specimen is a suspension on a grid or an ultrathin slice that is less than 100 nm thick. As the beam passes through the specimen, a picture is created as a result of the electrons' interactions with it. An imaging device, such as a fluorescent screen, a sheet of photographic film, or a sensor like a scintillator linked to a charge-coupled device, is then used to magnify and focus the image.

The operating modes of TEM instruments include diffraction, spectroscopy, scanning TEM imaging (STEM), conventional imaging, and combinations of these. There are numerous fundamentally diverse ways that contrast is formed, or "image contrast processes," even within conventional imaging. Contrast can result from position-to-position variations in thickness or density (referred to as "mass-thickness contrast"), atomic number (referred to as "Z contrast" using the standard abbreviation for atomic number Z), crystal structure or orientation (referred to as "crystallographic contrast" or "diffraction contrast"), the slight quantum-mechanical phase shifts that individual atoms produce in electrons that pass through them (referred to as "phase contrast"), the energy lost by electrons. Depending on the contrast mechanism as well as how the microscope is used—the settings of the lenses, apertures, and detectors—each mechanism provides the operator with a different kind of information. This means that a TEM is capable of returning a remarkable array of nanometer- and atomic-resolution data, and in ideal instances reveals not only the locations of all atoms but also the kind of atoms they are and the types of bonds they form with one another. Because of this, TEM is recognized as a crucial technique for nanoscience in the disciplines of biology and materials.

Components of HRTEM :

A HRTEM is made up of a number of parts, including an electron emission source for creating the electron stream, an electron vacuum system in which the electrons move, a number of electromagnetic lenses, and electrostatic plates. The last two let the user direct and control the beam anyway they see fit. A mechanism that enables the insertion, movement, and removal of specimens from the beam path is also necessary. The electrons that escape the system are then utilised to generate an image using imaging devices.



Figure 2.2: **FESEM (FEI Tecnai TEM.)**

2.2 Phase or Crystallographic characterization :

The main instrument involved in phase or crystallographic characterization is X-ray Diffraction. It operates with X-Ray to determine the phase of the sample. Apart from that, it is also possible to get information about the crystallographic planes, interplanar distance, crystal size and the lattice structure of the prepared sample.

2.2.1 X-Ray Diffraction (XRD):

X-rays are a form of electromagnetic radiation that has high energies and short wavelengths on the order of the atomic spacing for solids. When a beam of x-rays impinges on a solid material, a portion of this beam will be scattered

in all directions by the electron associated with each atom or ion that lies within the beam's pathway. Let us now examine the necessary conditions for diffraction of X-rays by a periodic arrangement of atoms. Diffraction occurs when a wave encounters a series of regularly spaced obstacles that are capable of scattering the wave and have spacing that are comparable in magnitude to the wavelength. Furthermore, diffraction is a consequence of specific phase relationships established between two or more waves that have been scattered by the obstacles. The phase relationship between the scattered waves, which will depend upon the difference in path length is important. One possibly results when its pathway length is an integral number of wavelengths.

Brag's Law :

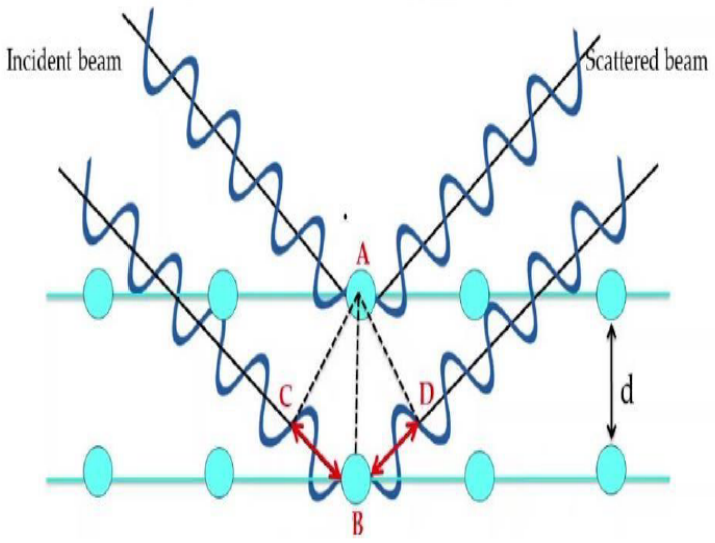


Figure 2.3: **FESEM (Brag's Law of diffraction**

Considering the two parallel planes of atoms, which have the same h, k and l Miller indices and are separated by the interplanar spacing d. Now assuming a parallel, monochromatic and coherent (in-phase) beam of x-rays of wavelength λ is incident on these two planes at an angle of Θ. Two rays in this beam are scattered by atoms A and B. Constructive interference of the scattered waves occur also an angle of Θ to the planes, if the path length

difference (i.e. CB+BD) between these waves is equal to a whole number, n, of wavelengths. So, the condition for diffraction is

$$\begin{aligned} n\lambda &= CB + BD \\ or, n\lambda &= dSin\Theta + dSin\Theta \\ or, n\lambda &= 2dSin\Theta \end{aligned}$$

Production of X-Ray :

X-rays are produced by bombarding a metal target (e.g., Cu, Mo usually) with a beam of electrons emitted from a hot filament (often tungsten). The incident beam will ionize electrons from the K-shell (1s) of the target atom and X-rays are emitted as the resultant vacancies are filled by electrons dropping down from the L (2p) or M (3p) levels. This gives rise to K_α and K_β lines.

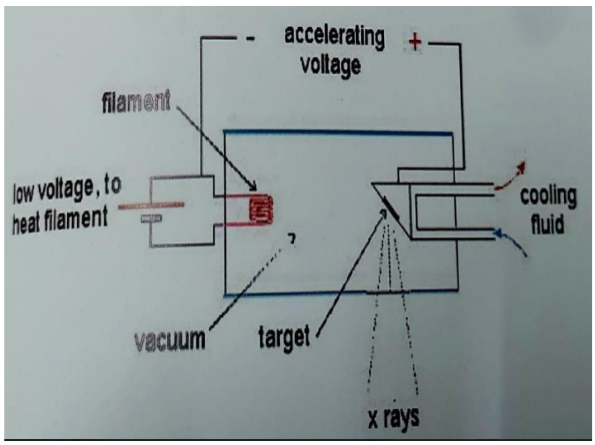


Figure 2.4: **Production of X-Rays.**

Particle Size determination by Scherrer's formula :

Experimentally obtained diffraction patterns of the sample are compared with the standard powder diffraction files published by the JCPDS. The



Figure 2.5: **X-Ray Diffraction (Bruker D8 advance.)**

average grain size of the samples was calculated using Scherrer's formula:

$$D = \frac{0.9\lambda}{\beta.Cos\theta}$$

Where, λ is the wavelength of x-rays,
And β is the full width at half maximum intensity in radians.
It is important to realize that the Scherrer's formula provides a lower bound on the particle size. The reason behind this is that a variety of factors can contribute to the width of a diffraction peak; besides particle size, the most important of these are actually is dependent on the factors like inhomogeneous strain and instrumental errors. If all of these other factors contributing to the peak width were zero, then the peak width would be determined solely by the particle size and the Scherrer's formula would apply. If the other contributors to the peak width is non-zero, then the particle size can be larger than the predicted by this formula, with the "extra" peak width coming from the other facts.

2.3 Spectroscopic Characterization :

2.3.1 UV-VIS near Infrared Spectroscopy:

The optical transmittance, absorbance, and reflectance in the ultraviolet-visible spectral area are measured using UV-Vis-NIR Spectrophotometers. Measurements of optical transmittance, absorbance, and reflectance in the ultraviolet visible spectral area are made using UV-Vis near Infrared (UV-Vis-NIR) Spectrophotometers. The amount of radiation that is absorbed, transmitted, or reflected at each wavelength is quantified using UV-Vis absorption spectroscopy. Typically, this is done by measuring the absorption while scanning the wavelength range. To determine the degree of multiple bond or aromatic conjugation within molecules, it is frequently employed in organic chemistry. The method can be expanded to include gases and solids as well as go beyond absorption to measure reflected light as opposed to transmitted light.
Light absorption can be described by two fundamental laws as:

Lambert's Law :

The proportion of incident light absorbed by a transparentmedium is independent of the intensity of the light (provided that there is no otherphysical or chemical change to the medium). Therefore, successive layers of equal thickness will transmit an equal proportion of the incident energy.
Lambert's law can be expressed by

$$\frac{I}{I_0} = T$$

Where I is defined as the intensity of transmitted light, I_0 is defined as intensity of incident light and T is the transmittance.

Beer's Law :

The absorption of light is directly proportional to both the concentration of the absorbing medium and the thickness of the medium in the light path.
A combination of the two laws (known jointly as the Beer-Lambert Law) defines the relationship between absorbance (A) and transmittance (T).

$$A = log\frac{I}{I_0} = log\frac{100}{T} = \varepsilon.c.b$$

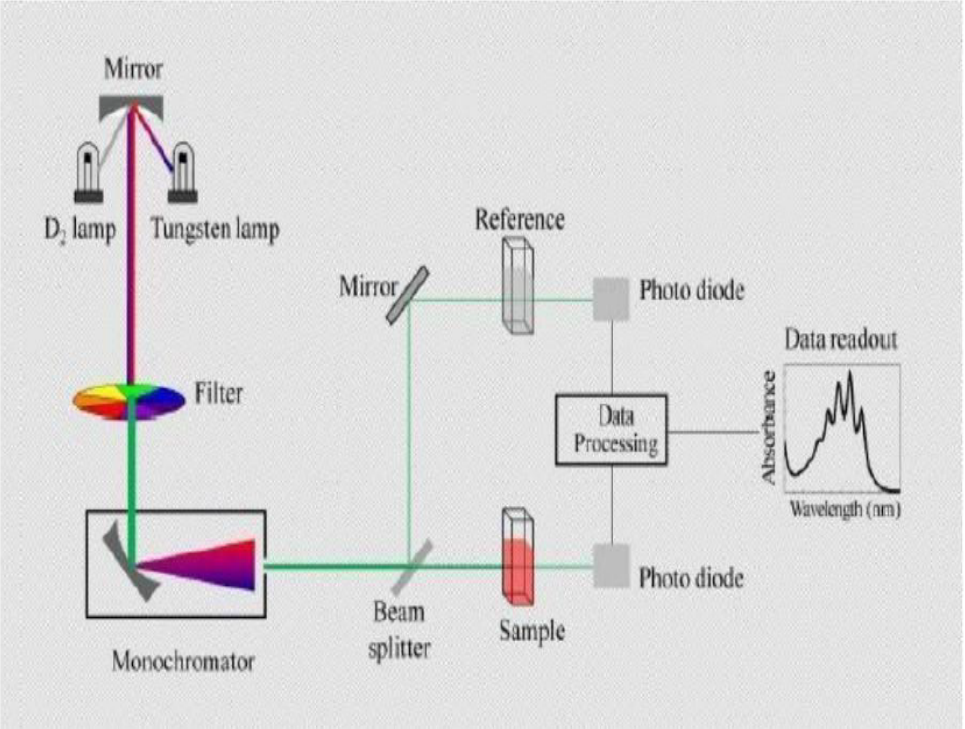


Figure 2.6: **Production of X-Rays.**

Where, A is absorbance, ε is molar absorptivity, c is molar concentration and b is path length.

2.3.2 Fourier Transform Infra-Red Spectroscopy :

For studying the vibrational properties of synthesised materials, FTIR spectroscopy is a very useful tool. The band positions and absorption peak of thin films are influenced not only by their chemical composition and structure, but also by their morphology.
The preferred method of infrared spectroscopy is known as Fourier Transform InfraRed (FT-IR). Infrared spectroscopy involves passing IR radiation through a sample. The sample absorbs some of the infrared radiation and passes some of it through (transmitted). The resulting spectrum depicts the sample's molecular absorption and transmission, resulting in a molecular fingerprint. No two unique molecular structures produce the same infrared

spectrum, just like a fingerprint. As a result, infrared spectroscopy can be used for a variety of purposes.

Why FTIR :

In order to overcome the limitations of dispersive instruments, Fourier Transform Infrared (FT-IR) spectrometry was developed. The slow scanning process was the main issue. It was necessary to develop a method for measuring all infrared frequencies simultaneously rather than individually. An interferometer, a very simple optical device, was used to develop a solution. The interferometer generates a unique signal that contains all of the infrared frequencies "encoded." The signal can be measured very quickly, usually in a fraction of a second. As a result, the time element per sample is reduced from several minutes to a few seconds. A beam splitter is used in most interferometers to divide the incoming infrared beam into two optical beams.

A flat mirror, which is fixed in place, reflects one beam. The other beam reflects off a flat mirror that moves a very short distance (typically a few millimetres) away from the beam splitter thanks to a mechanism. When the two beams meet again at the beam splitter, they reflect off their respective mirrors and are recombined. The signal that exits the interferometer is the result of these two beams "interfering" with each other because one beam's path is fixed and the other's is constantly changing as its mirror moves.

The resulting signal is known as an interferogram, and it has the unique

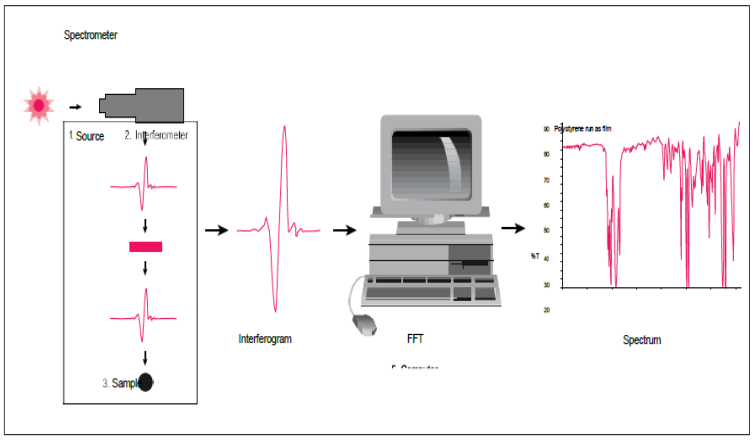


Figure 2.7: **Process of generating an FTIR spectra.**

property of having information about each infrared frequency that comes

from the source in every data point (a function of the moving mirror position) that makes up the signal. This means that all frequencies are measured simultaneously as the interferogram is measured. As a result of the interferometer's use, measurements are extremely quick. The measured interferogram signal cannot be interpreted directly because the analyst requires a frequency spectrum (a plot of the intensity at each individual frequency) in order to make an identification. It's necessary to have a way of "decoding" the individual frequencies. The Fourier transformation, a well-known mathematical technique, can be used to accomplish this. The computer performs this transformation and then presents the user with the desired spectral information for analysis.

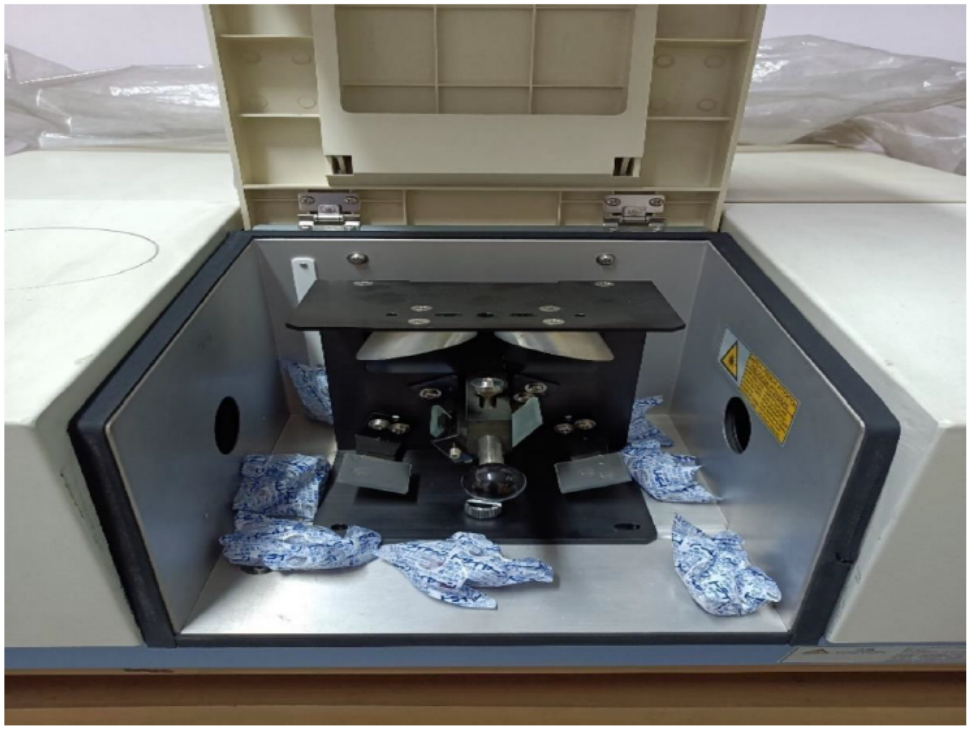


Figure 2.8: **Internal components of FTIR instrument.**

2.4 I-V Characterization :

The techniques for the measurement of the electrical behavior of laminated composites are the two- probe method and four probe methods. The two-probe method is based on the definition of resistance when two electrodes are used to measure the electrical resistance. Figure below shows a specimen, on which a pair of contacts (probe 1 and probe 2) with conductive wires is attached. Two probes are used for the electrical current input, as well as for the voltage measure. The resistance of the segment between the voltage contacts can be calculated through Ohm's law:

$$V = R*I$$

where, V and I are the voltage and current from the voltage and current contacts, respectively.



Figure 2.9: **Two probe device used in the project.**

Bibliography

[1] Thermo Nicolate, Introduction to Fourier Transform Infrared Spectrometry, © 2001 Thermo Nicolet Corporation

[2] Kortüm, G. Reflectance Spectroscopy: Principles, Methods, Applications; Kortüm, G., Ed.; Springer: Heidelberg/Berlin, Germany, 1969.

[3] Frei, R.W.; Frodyma, M.M.; Lieu, V.T. Diffuse reflectance spectroscopy. In Instrumentation for Spectroscopy. Analytical Atomic Absorption and Fluorescence Spectroscopy. Diffuse Reflectance Spectroscopy; Svehla, G., Ed.; Wilson and Wilson's Comprehensive Analytical Chemistry; Elsevier Scientific Publishing Company: Amsterdam, The Netherlands, 1975; Volume 4, Chapter 3, pp. 263–345.

[4] Frei, R.W.; Frodyma, M.M.; Lieu, V.T. Diffuse reflectance spectroscopy. In Instrumentation for Spectroscopy. Analytical Atomic Absorption and Fluorescence Spectroscopy. Diffuse Reflectance Spectroscopy; Svehla, G., Ed.; Wilson and Wilson's Comprehensive Analytical Chemistry; Elsevier Scientific Publishing Company: Amsterdam, The Netherlands, 1975; Volume 4, Chapter 3, pp. 263–345.

[5] Photoluminescence Spectroscopy, Physics U600, Adv Lab I – Physics of Waves and Optics – Summer 2004, D. Heiman, North eastern University, 6/1/2004.

Chapter 3

Literature Review:

3.1 Synthesis Technique :

These days, the industry is very interested in carbonaceous materials including graphite, graphene, graphene oxide (GO), and reduced graphene oxide (rGO) because of their vast array of potential uses in several emerging technology domains. These materials have a rich 150-year synthetic history. Over time, the process of synthesizing these materials improved, resulting in increased manufacturing volume and reduced risks. To create graphene oxide (GO) from graphite and subsequently reduce it to rGO, there are several synthesis methods. Three primary methods for making graphene oxides have been identified in the past: The Staudenmaier (ST) process, which fumes nitric acid using a chlorate oxidant; the Hofmann (HO) version, which uses sulfuric acid and chlorate; and the Hummers' (HU) method, which makes use of an oxidant permanganate. This chapter discusses the synthesis of GO using the ST method and Hummer's method. This previously created GO can be used to produce the rGO through a hydrothermal procedure. In this chapter, the hydrothermal process is also briefly described.

In order to control different aspects of the Si structures, a multitude of techniques have been developed to fabricate Si nanostructures using top-down or bottom-up approaches. These techniques include chemical vapor deposition (CVD), reactive ion etching (RIE), electrochemical etching, solution-liquid-solid (SLS) process, vapor-liquid-solid (VLS) growth, and molecular beam epitaxy (MBE). This chapter contains a detailed discussion of two techniques: the VLS process and Chemical Etching.

3.1.1 GO synthesis using Staudenmaier's (ST) method:

Materials : Graphite, concentrated sulphuric acid (H2SO4), Sodium Nitrate (NaNO3), Hydrogen peroxide (H_2O_2) and Potassium Permanganate ($KMnO_4$).
Process :

1. In order to scatter the graphite into the solution, the reaction is initiated by first stirring it with H2SO4 in a reaction flask for a few minutes at 0° C.
   itemAfter that sodium nitrate is added to the mixture in some portions and kept it for 1 hour under stirring.

2. The temperature of the mixture eventually rises to 900 C when potassium permanganate is gradually added at 350°C. For the following hour, the temperature remains constant.

3. Extra water is added to the solution followed by pouring of H_2O_2.

4. Once the solution ends it reaction, it is washed multiple times with warm water.

5. To separate the solid GO, the mixture was then centrifuged multiple time and the solid GO is collected.

6. The solid GO then dried in vacuum oven for some days before use.

3.1.2 Hydrothermal Process :

According to definitions found in the literature [1], hydrothermal synthesis is a closed-loop method wherein all chemical reactions occur at elevated temperatures and pressures greater than atmospheric pressure (P ¿ 101,325 Pa) in a water solvent. Scholars have frequently modified this definition. For example, Byrappa and Yoshimura [2] defined a "hydrothermal reaction" as any heterogeneous chemical reaction that occurs in a closed system above room temperature and at a pressure greater than 1 ATM while a solvent, whether aqueous or not, is present. In this review, we will assume that "hydrothermal synthesis" refers to a process that takes place in an aqueous environment (where mH2O ¿ 50%) at a pressure that is either higher than or equivalent

to atmospheric pressure. In hydrothermal processes, reaction products are mainly oxides and salts due to the properties of water as a solvent.

One technique for creating a wide range of materials, including metals, semiconductors, ceramics, and polymers, is called solvothermal synthesis. The procedure uses a solvent that promotes precursor interaction during synthesis at moderate to high pressure (usually between 1 ATM and 10,000 ATM) and temperature (usually between 100°C and 1000°C). The process is known as "hydrothermal synthesis" if water is utilized as the solvent. Hydrothermal synthesis is often carried out below the water's supercritical temperature (374°C). The procedure can be used to create materials with a variety of morphologies, such as bulk powders, single crystals, thin films, and nanocrystals.

Advantages of Hydrothermal method :

1. Possible to precipitate powders directly from solution
2. Ability to synthesize crystals of substances which are unstable near melting point.
3. Suitable when it is difficult to dissolve precursors at room or lower temperatures.
4. Can be hybridised with other processes like microwave, ultrasound etc. [2]

Disadvantages of Hydrothermal method :

1. High cost of equipment e.g., the need of expensive autoclaves.
2. Inability to observe the crystals in the process of their growth.[3,4]

• Reduction of rGO from GO :

Using a hydrothermal process, the generated graphene oxide (GO) can be further reduced to eliminate the majority of its edge-linked functionalization groups, resulting in a pure layer of graphene oxide with fewer groups (which is ultimately referred to as reduced graphene oxide). Because hydrothermal or solvothermal techniques maintain a steady temperature and pressure, they

can efficiently reduce material in a shorter amount of time. In addition to reduction, doping is an additional step in the hydrothermal process. Reduction agents can be various amide groups, sulfur groups, etc.

In this project work, modified Hummer's method is being used for producing good quality of graphene oxide (GO), rGO and GQD are synthesised using hydrothermal process.

3.2 Review of Photonic Synapses :

3.2.1 Perovskite/Organic semiconductor based Photonic Synapses :

This paper[7] illustrate the performance of $CsPbBr_3$ quantum dots perovskite with an organic semiconductor (poly[2,5-(2-octyldodecyl)- 3,6-diketopyrrolop--yrrole-alt-5,5-(2,5-di(thien-2-yl)thieno [3,2-b]thiophene)], DPPDTT), as the photonic synapse. The composite of DPPDTT/$CsPbBr_3$ enhance the mobility performance under very low voltage rate. After doing the all necessary characterization they started to study different memory operations like ΔEPSC, PPF. plasticity i.e. transition from LTP to STP, learning experience and also they had performed AND, OR optical gate in their synaptic device.

3.2.2 Ferroelectric van dar waals heterostruture based Photonic Synapses :

The authors have been used In_2Se_2 ferroelectric material with in and out phase planes which was controlled by the gate voltage. Their device has a perfect architecture of an top gate FET. They studied the synaptic performance in a very detail and variative manner like they varied the pulse numbers, pulse width different intensity of pulses, AND, OR operations etc. There are several Perovskite, ferroelectric, 2D transitional materials and their compositions with other substance have been studied so far.

Bibliography

[1] Henglein, A. Small-particle research-physicochemical properties of extremely small colloidal metal and semiconductor particles. Chem. Rev. 1989, 89, 1861–1873.

[2] K. K. Sadasivuni, D. Ponnamma, S. Thomas and Y. Grohens, Evolution from graphite to graphene elastomer composites, Prog. Polym. Sci., 2014, 39(4), 749–780.

[3] K. Deshmukh, M. B. Ahamed, S. Sankaran, S. K. K. Pasha, K. K. Sadasivuni, D. Ponnamma and M. A. A. AlMaadeed, Studies on the mechanical, morphological and electrical properties of highly dispersible graphene oxide reinforced polypyrrole and polyvinyl alcohol blend composites, Mater. Today: Proc., 2018, 5, 8744–8752.

[4] K. Deshmukh, S. Sankaran, M. B. Ahamed, S. K. K. Pasha, K. K. Sadasivuni, D. Ponnamma and M. A. A. AlMaadeed, Studies on the electrical properties of graphene oxide reinforced poly(4-styrene sulfonic acid) and polyvinyl alcohol blend composites, Int. J. Nanosci., 2018, 17, 1760005–1760013.

[5] Namdari P., Negahdari B., Eatemadi A. Synthesis, properties and biomedical applications of carbon-based quantum dots: An updated review. Biomed. Pharmacother. 2017;87:209–222. doi: 10.1016/j.biopha.2016.12.108.

[6] Zhou J., Shan X., Ma J., Gu Y., Qian Z., Chen J., Feng H. Facile synthesis of P-doped carbon quantum dots with highly efficient photoluminescence. RSC Adv. 2014;4:5465–5468. doi: 10.1039/c3ra45294h.

[7] "Perovskite/Organic Semiconductor-Based Photonic Synaptic Transistor for Artificial Visual System" Dandan Hao, Junyao Zhang, Shilei Dai, Jianhua Zhang, and Jia Huang; ACS Appl. Mater. Interfaces 2020

[8] Photonic synaptic transistor based on p-type organic semiconductor blending with n-type organic semiconductor; https://doi.org/10.1109/LED.2021.3090906

[9] On-chip photonic synapse; SCIENCE ADVANCES 27 Sep 2017 Vol 3, Issue 9 DOI: 10.1126/sciadv.1700160

[10] Artificial Visual Systems Fabricated with Ferroelectric van der Waals Heterostructure for In-Memory Computing Applications; ACS Nano 2023, 17, 21, 21297–21306

Chapter 4

Synthesis of Materials:

4.1 Synthesis of GO using modified Hummer's method :

- **Materials Used :**

Graphite flakes (7-10 μm grain size, 99% purity) from Alfa Aesar,sodium chloride (NaCl), 99% purity), sulfuric acid (H_2SO_4, 98% by weight, G.R.), potassium permanganate ($KMnO_4$, 99% purity), hydrochloric acid (HCL), hydrogen peroxide (H_2O_2, 30% by weight, A.R.) from Merck were used for synthesis. Deionized (DI) water was taken from a Direct-Q Millipore deionized (18 ohm at 25°C).

- **Procedure :**

1. At the initial phase of synthesis of materials 3 gm of graphaite power and 3 gm of NaCl have been taken into a morter and petis for grinding around 2 hours. Then 98% of H_2SO_4 has been added to the grinded version of graphite and NaCL mixture and left it in stirring for 30 mins.

2. Next, 10 gm $KMnO_4$ has been added as an oxidizing agent in a continuous stirring condition at 15^{circ}C. The mixture was allowed to stir for 6 hours.

3. After 6 hours 200 mL of DI and 30% ofHydrogen peroxide (H_2O_2) has been added to the mixture for the termination of the reaction and left

for some time for cooling down the temperature. Whole mixture has been aged to the magnetic stirring for 24 hours.

4. Next, the mixture has been divided into 6 different 40 mL centrifuge tube for the cleaning procedure. To complete the centrifugation hydrochloric acid (HCl) and DI water have been used alternatively for properly cleaning the solution. A last, the centrifugation machine set at 4500 rpm for 15 mins. to reduce the p^H level of the solution at 7 which has been done after 3 repetition of centrifugation.

5. Lastly, the solution has been dried in an oven at 60°C for 24 hours. Finally, the Graphene Oxide (GO) is completely prepared.

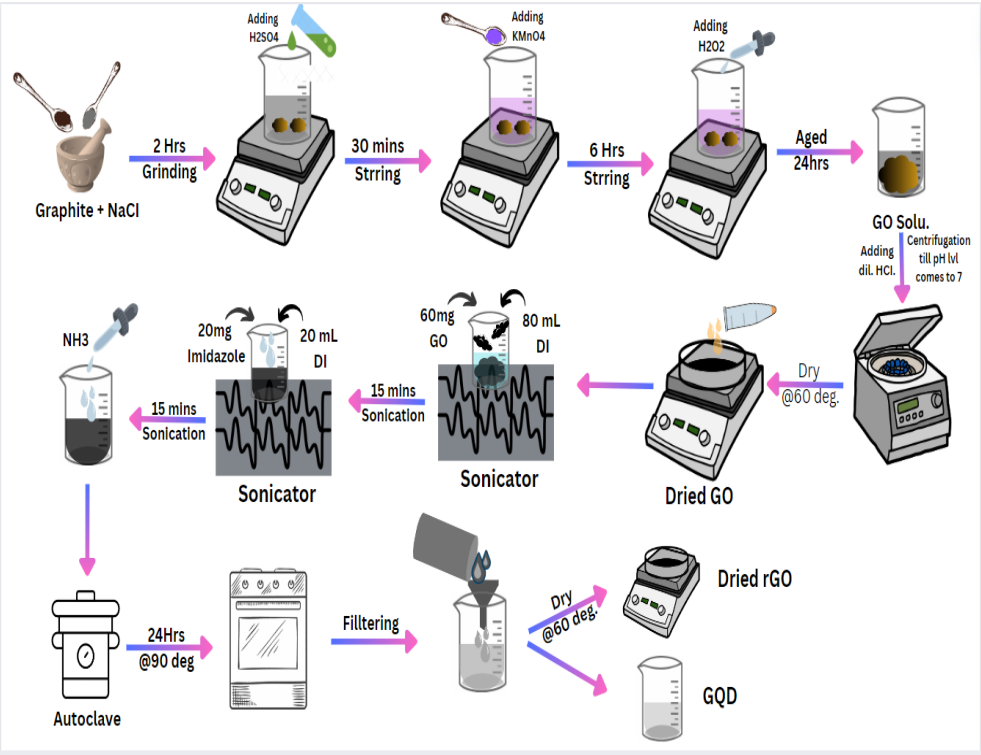


Figure 4.1: **Schmatic of Synthesis Procedure of GO,rGO and GQD.**

4.2 Synthesis of rGO and GQD using Hydrothermal Method :

- **Materials Used :**

Graphene Oxide (GO) prepared using modified Hummer's method, Imidazole, ethanol (C_2H_5OH, 99% pure), ammonia solution (NH_4OH, 25% by weight), Teflon.

- **Procedure :**

1. For preparing Reduced Graphene Oxide (rGO), firstly 60 mg of prepared GO with 80 mL of DI water were taken into a beaker and leave it for sonication about 15 mins for GO dispersion.

2. Afterwards, 20 mL of Imidazole and 20 mL of DI water are poured into the mixture where Imidazole used as the reducing agent.

3. Again the mixture left for sonication about 15 mins. Then Ammonia (NH_3) is being added to the solution. At last the whole mixtured solution has been taken into two autoclaves and put it into the oven for 24 hours at 90°C.

4. At final stage the solution was filtered, the filtrate substance dried at 60°C for 24 hours which we got as 2D material of rGO and the residue from the filtration is Graphene quantum dot (GQD).

Bibliography

[1] A. K. Geim, K. S. Novoselov, Nat. Mater. 2007, 6, 183 –191.

[2] C. K. Chua, M. Pumera, Chem. Soc. Rev. 2013, 42, 3222– 3233; b) M. Pumera, Electrochem. Commun. 2013, 36, 14 –18. L. Staudenmaier, Ber. Dtsch. Chem. Ges. 1898, 31, 1481 –1487.

[3] U. Hofmann, E. König, Z. Anorg. Allg. Chem. 1937, 234, 311 –336.

[4] W. S. Hummers, R. E. Offeman, J. Am. Chem. Soc. 1958, 80, 1339 –1339.[8] C. K. Chua, Z. Sofer, M. Pumera, Chem. Eur. J. 2012, 18, 13453 – 13459.

[5] A. Y. S. Eng, A. Ambrosi, C. K. Chua, F. S˘ane˘k, Z. Sofer, M. Pumera, Chem. Eur. J. 2013, 19, 12673 –12683 ; b) D. C. Marcano, D. V. Kosynkin, J. M. Berlin, A. Sinitskii, Z. Sun, A. Slesarev, L. B. Alemany, W. Lu, J. M.Tour, ACS Nano 2010, 4, 4806 – 4814.

[6] C. K. Chua, M. Pumera, Chem. Asian J. 2012, 7, 1009 –1012.[11] Y. Si, E. T. Samulski, Chem. Mater. 2008, 20, 6792 –6797.

[7] Y. Wang, S. Gao, X. Zang, J. Li, J. Ma, Anal. Chim. Acta 2012, 716, 112 –118.

[8] S. T. Yang, S. Chen, Y. Chang, A. Cao, Y. Liu, H. Wang, J. Colloid Interface Sci. 2011, 359, 24 –29.

[9] M. Giovanni, H. L. Poh, A. Ambrosi, G. Zhao, Z. Sofer, F. Sanek, B. Khezri, R. D. Webster, M. Pumera, Nanoscale 2012, 4, 5002– 5008.

[10] J. L. Li, K. N. Kudin, M. J. McAllister, R. K. Prud'homme, I. A. Aksay, R. Car, Phys. Rev. Lett. 2006, 96, 176101.

Chapter 5

Characterization of Materials:

This chapter has covered a variety of material characterizations that were created using the hydrothermal synthesis method. The morphological characterisation and it's analysis will be covered first in this chapter, followed by crystallographic characterization and analysis, and finally optical or spectroscopic characterization and analysis.

5.1 Morphological Characterization & Analysis :

This section of my thesis work involves mainly two types of morphological characterization for two different type of materials. Those are field emission scanning electron microscopy (FESEM) and high-resolution transmission electron microscopy (HRTEM). The fundamental morphological structure of nanoparticles or nanosheets in the 500 nm–5 μm range is described by the FESEM image. On the other hand, the HRTEM image offers details regarding the morphological characteristics of the nanoparticles in the 5–100 nm range.

5.1.1 Field Emission Scanning Electron Microscopy (FESEM) of rGO :

Reduced graphene oxide is having almost same morphology as graphene oxide or graphene which refers to the nano-structure of 2D nanomaterials. Their

main morphological structure resembles a layered or sheet-like structure.

The RGO micrograph shown in the image shows the results of chemical

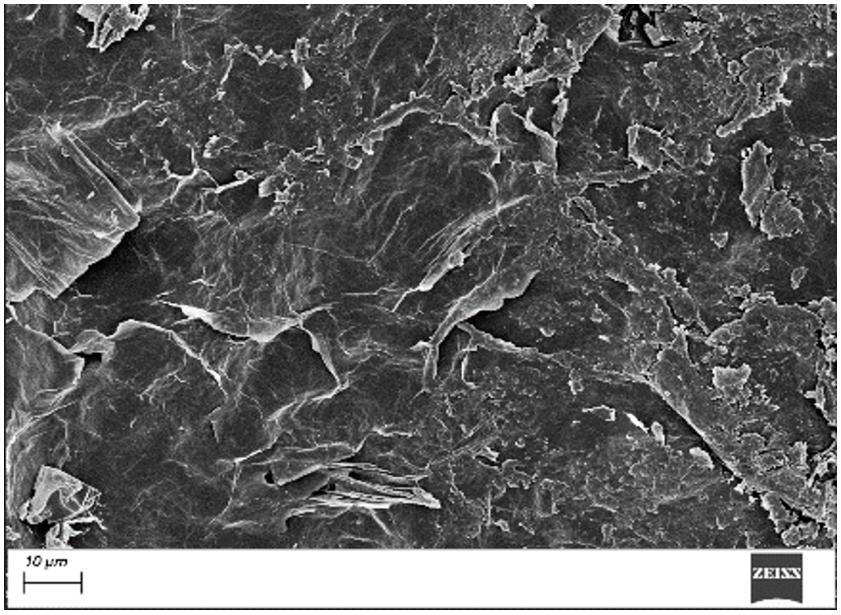


Figure 5.1: **FESEM Image of rGO.**

reduction using imidazole. Crumpled thin sheets were present on the RGO surface, and these collected to produce disordered structural material.

5.1.2 High-resolution transmission electron microscopy (HRTEM) of GQD :

An HRTEM image of a GQD created using a modified version of Hummer's technique is displayed. The tiny, spherically-shaped structures verify that GQD is present. The products contained consistently distributed, tightly packed GQDs, ranging in diameter from 5 to 15 nm.

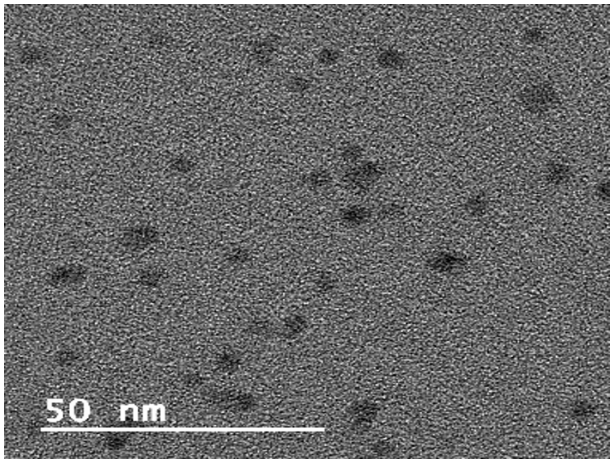


Figure 5.2: **HRTEM Image of GQD.**

5.2 Crystallographic Characterization & Analysis :

It is crucial to perform X-Ray Diffraction (XRD) on the samples in order to determine their crystallographic nature, including crystal structure, lattice structure, and interplanar spacing. X-ray diffraction (XRD) was used in this experiment to analyze reduced graphene oxide and graphene quantum dots that were produced hydrothermally.

5.2.1 X-Ray Diffraction of rGO & GQD :

Bragg's law of diffraction serves as the foundation for the operation of the XRD instrument. It provides details on the material's crystal type, including its crystalline or amorphous structure and the distance between its two lattice planes. Initially, the JCPDS database was consulted to compare sample's peak XRD plot in order to determine whether or not the substance that was synthesized in this experiment was reduced graphene oxide or not. The average peak angle (2Θ) is equivalent to the JCPDS database record to confirm the products are rGO only.

XRD pattern of GQD shows two peaks at 27.06° and 27.27 ° which indicates the lattice plane of (002) and (100) respectively [4]. The second less intense

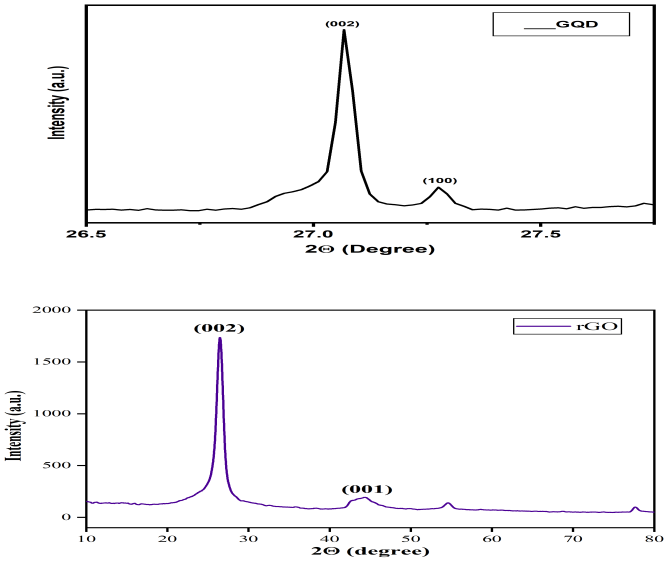


Figure 5.3: **XRD Plot of GQD.**

peak refers for un-reacted graphite. At rGO case it has a perfect intense peak at 26.44 ° which refers (002) lattice phase of rGO and the sharp peak indicates the removal of oxygen groups after reduction process. Another less intense peak can be seen at 2θ =44.64° with (001) orientation which attributed by the turbostratic band of disordered carbon materials.

5.3 Spectroscopic Characterization & Analysis :

This portion of thesis only talks about the optical performance of the synthesized materials. We will discuss the photo-luminascene, fluorescent and excitation properties of the materials.

5.3.1 UV-Vis Spectroscopy of rGO & GQD:

Ultraviolet-visible spectroscopy uses light from the visible and nearby ranges to analyze reflectance and absorption in the ultraviolet and adjacent full visible areas of the electromagnetic spectrum. The perceived colors of the

compounds are directly impacted by their reflectance or absorption in the visible spectrum. Electronic transitions between atoms and molecules occur in this part of the spectrum. Fluorescence spectroscopy and absorption spectroscopy work well together. Whereas absorption deals with the transfer from the ground state to the excited state, fluorescence deals with the transition from the excited state to the ground state.

UV-Vis data from Tauc plot can also be used to evaluate the optical band gaps. The photon energy, hν, is usually plotted on the abscissa of a tauc plot, while the material's absorption coefficient, $(\alpha h\nu)^{\frac{1}{2}}$, is shown on the ordinate. After that, the energy of the amorphous material's optical bandgap can be calculated by extending this linear region to the abscissa.

In order to prepare the sample for UV Vis absorption , 1 mg of rGO was first taken in an appen-drop with 10 mL of N-Methylpyrrolidone (NMP). Then it is left for sonication about 30 mins for proper dispersion.

The residue of my synthesized material was sonicated for 10 minutes in order to analyze the GQD absorbtion analysis.

From [Fig 5.4, 5.5] the estimated wavelength in absorption edge for the

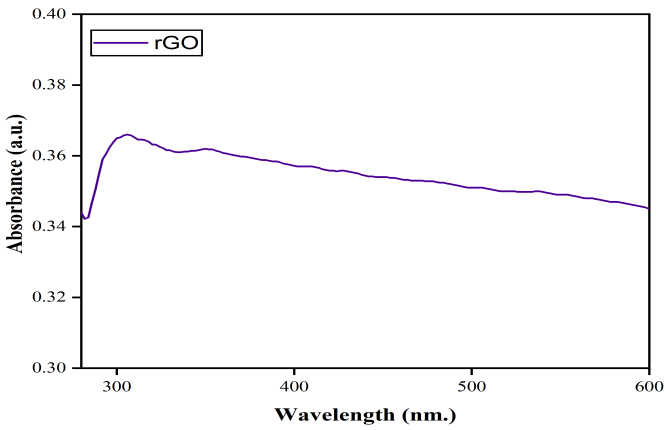


Figure 5.4: **UV-Vis Absorption Spectra of rGo**

spectra of rGO and GQD are 295 nm and 260 nm respectively. These absorption peaks indicates different electronic transitions; exact which bands

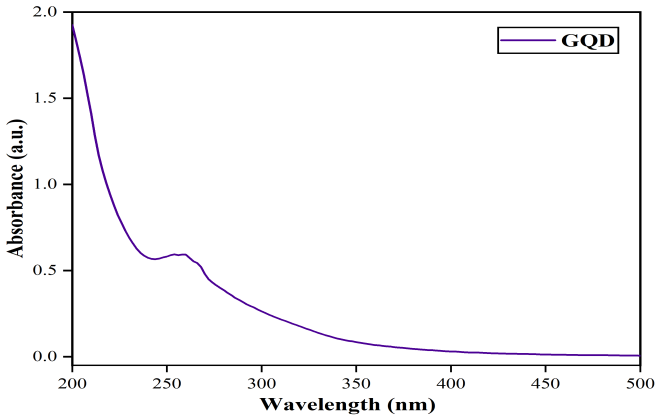


Figure 5.5: **UV-Vis Absorption Spectra of GQD.**

of transition occurs that is still in investigation.
Determining the materials' optical band gap is my main goal in this endeavor. In the near future, we may examine the heterostructure development of the aforementioned materials with the aid of band gap evaluation, and it will also assist me with band gap engineering, which is a crucial component of my research.

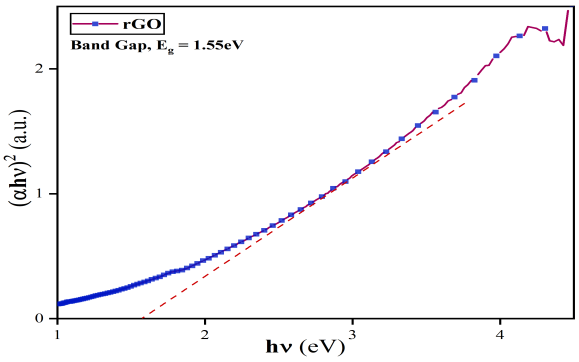


Figure 5.6: **Tauc plot and band calculation of rGO.**

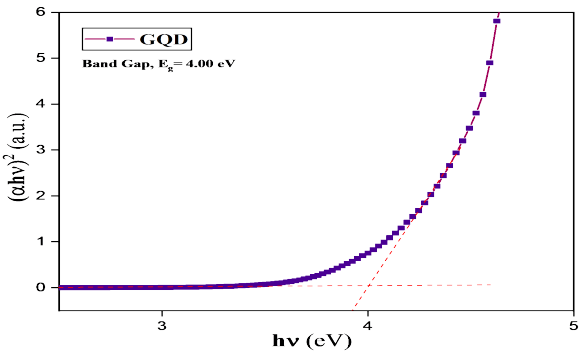


Figure 5.7: **Tauc plot and band calculation of GQD.**

The evaluated band gap from the Tauc's plots are 1.55eV and 4.00 eV. So, two of my sample are showing extreme different in band gap values which are my main point of intention for getting the memory function (discussed in later chapter).

5.3.2 Fourier Transform Infra-Red Spectroscopy (FTIR) of rGO :

Several oxygen functional groups, including carboxyl, epoxy, hydroxyl, and others, have been eliminated from the graphene plane through the reduction process of graphene oxide. The vibrational frequency of these groups is here provided using FTIR. Therefore, it is possible to verify that GO has been successfully reduced by examining the peaks and their strength. The study is predicated on the idea that molecular bonds are vibrationally excited when infrared light energy is absorbed within the 4000-1000 cm^{-1} wavelength. The peaks are observed at 3440, 2944, 2326, 1745, 1647, 1440 and 1330 cm^{-1} which corresponds O-H, C-H, C $\equiv$ N, C=C, C=N, C-O-C and C=O groups. It is clear from the the graph the peaks are quite low intense which describes the reduction of functional groups due to the presence of the reducing agent Imidazole.

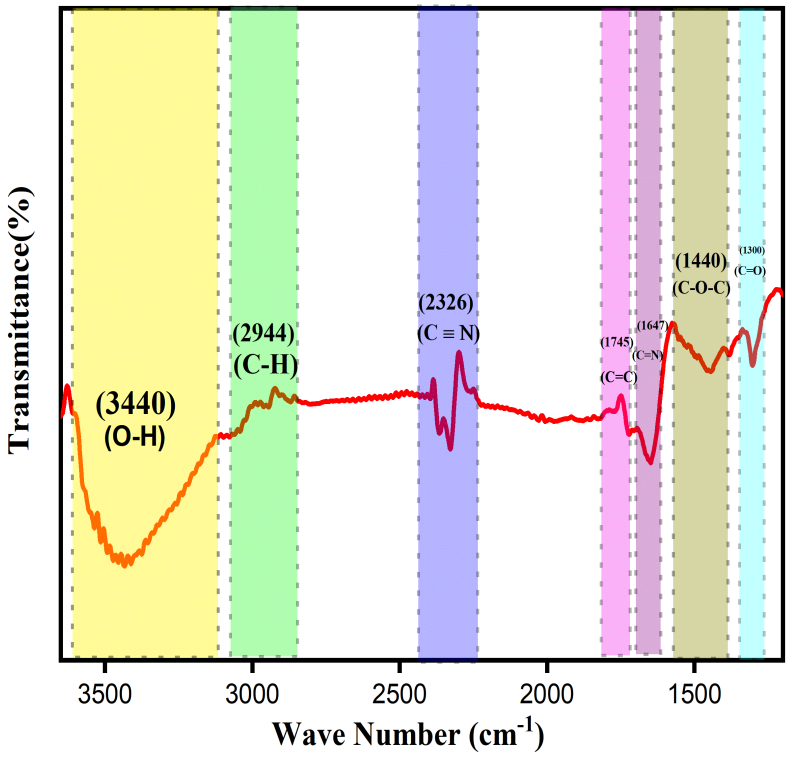


Figure 5.8: **FTIR Plot of rGO.**

5.3.3 Photo-luminescence (PL) of GQD :

This section describes the photo-luminescence and fluorescent properties of GQD. Our sample was irradiated with different wavelength value of illumination where our sample showing maximum at 320 nm.

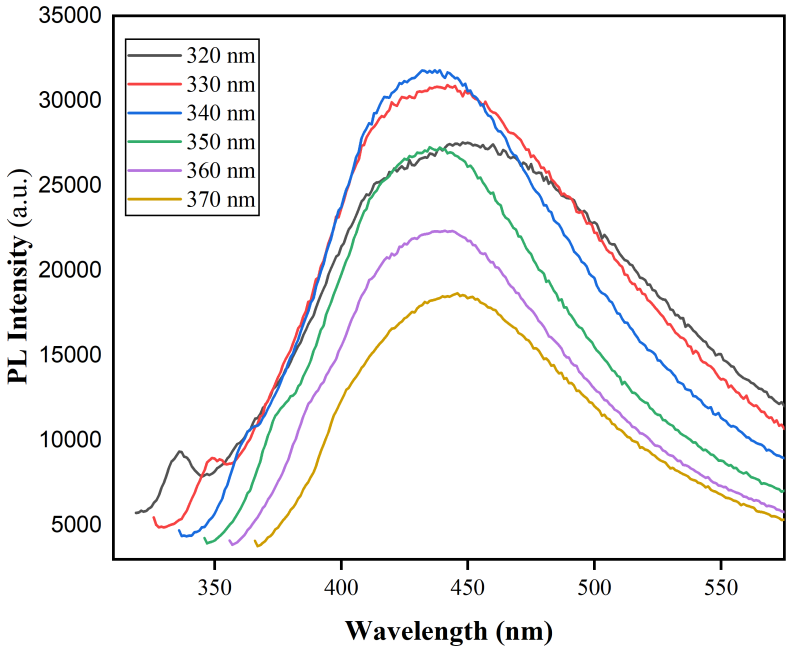


Figure 5.9: **PL plot of GQD.**

Bibliography

[1] J. Hou, Y. Shao, M. W. Ellis, R.B. Moore, B. Yi, Graphene-based electrochemical energy conversion and storage: fuel cells, supercapacitors and lithium ion batteries, Phys. Chem. Chem. Phys. (13) (2011) 15384-15402.

[2] G. Wu, K. L. More, C.M. Johnston, P. Zelenay, Polymer wrapping technique: an effective route to prepare Pt nanoflower/carbon nanotube hybrids and application in oxygen reduction Science,(332)(2011) 443–447. 4. W. Yang, Y. Wang, J. Li, X. Yang, Polymer wrapping technique: an effective route to prepare Pt nanoflower/carbon nanotube hybrids and application in oxygen reductionEnviron. Sci, (3)(2010) 144–149.

[3] C. Goswami, K. K.Hazarika, P.Bharali, Transition metal oxide nanocatalysts for oxygen reduction reaction,Materials Science for Energy Technologies, 2018.

[4] "Synthesis of graphene oxide and graphene quantum dots from miscanthus via ultrasound-assisted mechano-chemical cracking method" ; Yuxin Yan , Sivakumar Manickam , Edward Lester , Tao Wu , Cheng Heng Pang; https://doi.org/10.1016/j.ultsonch.2021.105519

[5] "Role of C–N Configurations in the Photoluminescence of Graphene Quantum Dots Synthesized by a Hydrothermal Route OPEN"; Scientific Reports 6(1):21042; http://dx.doi.org/10.1038/srep21042

[6] "Tuning the Photoluminescence of Graphene Quantum Dots through the Charge Transfer Effect of Functional Groups"; Sung Hwan Jin, Da Hye Kim, Gwang Hoon Jun, Soon Hyung Hong, and Seokwoo Jeon; https://doi.org/10.1021/nn304675g

[7] "Facile synthesis of graphene from graphite using ascorbic acid as reducing agent"; THE 3RD INTERNATIONAL CONFERENCE ON ADVANCED MATERIALS SCIENCE AND TECHNOLOGY (ICAMST 2015);http://dx.doi.org/10.1063/1.4945457

Chapter 6

Device Fabrication:

This chapter serves the basic procedure for the formation of a proper device to utilize I-V characteristics, checking responsivity and detectivity and also to get the optimization of the device.

- **Steps for Device Fabrication :**

1. The initial substrate used was a flexible Polyethylene terephthalate (PET) sheet coated with Indium tin oxide (ITO) which was cut into a dimension of 20 mm by 10 mm.

2. Next, a 5-mm-long Polytetrafluoroethylene (Teflon) jacket was put into each end of the substrate; this jacket served as a mask during the etching process. We employed chemical etching to remove ITO from the channel region with the help of HCl (35%). Afterwards we use DI water to wash the etched substrate.

3. For the preparation of material deposition at channel region, firstly we took N-Methylpyrrolidone (NMP) dispersive solution with rGO with a concentration ratio of 10:1 and left it for 30 mins for proper dispersion.

4. Next, we spin coat the material at the channel region for 30 seconds at a speed of 2500 rpm after dropping the dispersed rGO on it. Following the appropriate spin coating, the dispersive medium is allowed to evaporate on a hot plate that is set at 60°C for two minutes.

5. To obtain two layers of rGO for optimal mobility performance, we repeat the above step again.

6. Now for the construction of GQD layer , we again spin coat the liquid solution of GQD at channel region with same stipulated time and rpm. For the evaporation of the solvent we again use hot plate fixed at 100∘.

7. As we make a layer dependent memory functionalized device, we repeat step 5 upon our desire of fabrication.

Finally the total formation of our layer dependent device is shown in the Fig. 6.1.

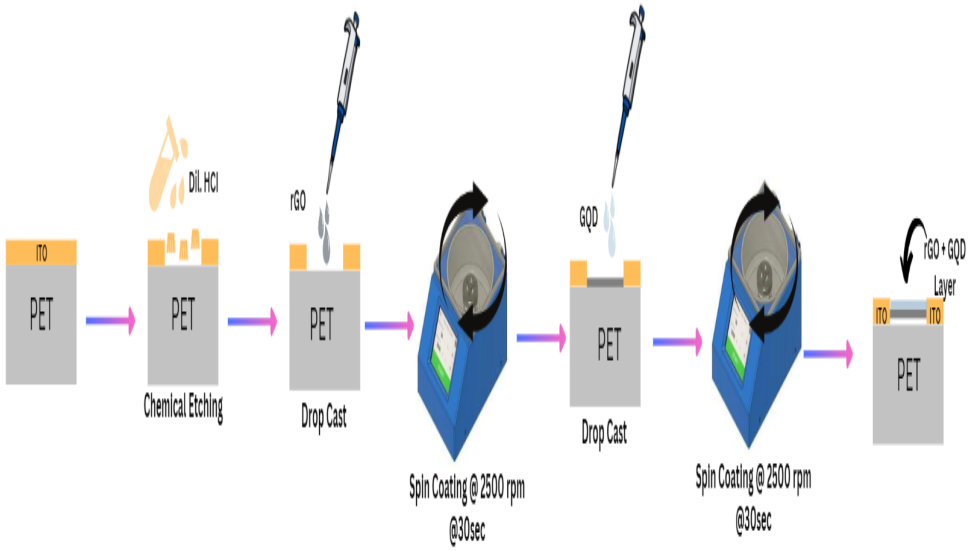


Figure 6.1: **Schematic of Device Fabrication.**

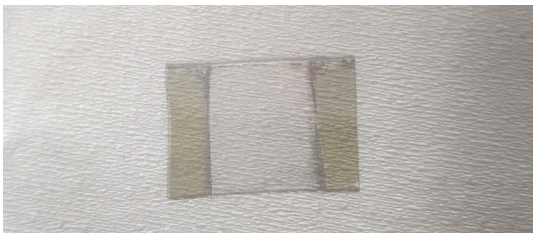


Figure 6.2: **Final Device.**

• **Device Optimization :**

We carefully optimize the channel region to obtain the correct surface area that it is intended to expose to light illumination. Initially, we periodically shortened the channel portion's length by 10 mm, 8 mm, 6 mm, 4 mm, and 2 mm. The device was then subjected to light irradiation for each shorter length. Next, we once more reduce the device's breadth channel in the same periodic manner and then also examined it's performance under the light irradiation.

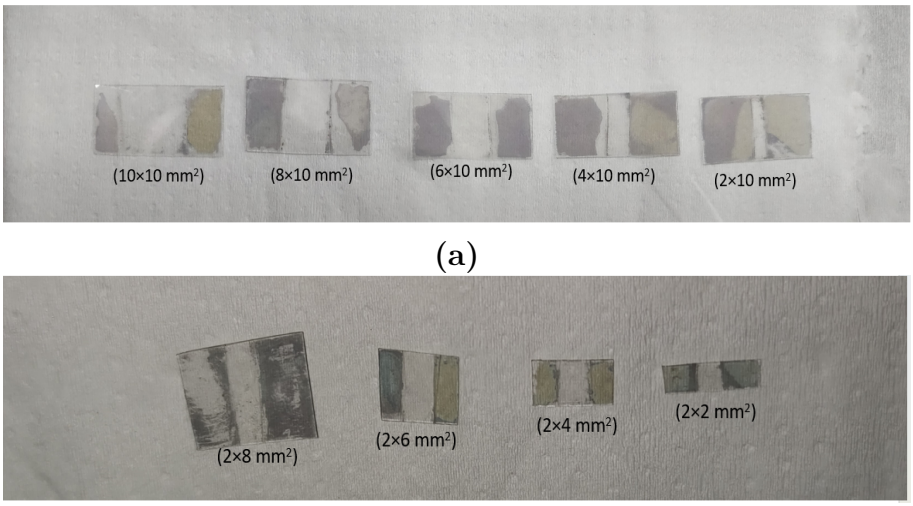


Figure 6.3: **Optimization of devices (a) Length-wise and (b) Breadth-wise.**

Bibliography

[1] "Perovskite/Organic Semiconductor-Based Photonic Synaptic Transistor for Artificial Visual System" Dandan Hao, Junyao Zhang, Shilei Dai, Jianhua Zhang, and Jia Huang; ACS Appl. Mater. Interfaces 2020

[2] "Artificial Visual Systems Fabricated with Ferroelectric van der Waals Heterostructure for In-Memory Computing Applications"; Biswajit Das, Sungpyo Baek, Jingjie Niu, Cheolhwa Jang, Yoonmyung Lee, Sungjoo Lee; ACS nano; American Chemical Society

[3] " NIR photodetector based on p-silicon nanowires/n-cadmium sulfide nanoscale junctions"; Ankita Chandra , Supratick Giri , Biswajit Das , Shrabani Ghosh , Sourav Sarkar , K.K. Chattopadhyay ; Applied Surface Science; https://doi.org/10.1016/j.apsusc.2021.149256

Chapter 7

Results and Discussion:

Eighty percent of external stimuli can be recognized by the human visual system; the other portion is completely destroyed by the external environment. The retina receives external optical information, and the individual memorizes picture impressions to construct their memories. Because of the tremendous advancements in artificial intelligence and smart robotics, researchers are focusing on artificial visual perception systems that, like the human visual system, are capable of detecting, processing, and memorizing information about the external environment. Light-stimulated artificial synaptic devices with fast propagation speed, low latency, and huge bandwidth have been designed to improve the efficiency of processing visual information since they can transform optical impulses directly into electrical signals.

7.1 Analysis of Device with Different Light Illumination :

The functionality of the device under various light irradiations is covered in this section. Here, we're employing four distinct light cases: visible, infrared, ultra violet, and dark wavelengths. The voltage range of the device is set to -2 V to +2 V; outside of this range, the device malfunctions and produces a significant quantity of noise. In order to determine the wavelength that is most highly absorbed, we decided to use the 10*10 mm^2 channel region based device.Since we are creating a layer-dependent memory device, we also

alter the device's layer numbers and evaluate how well it functions under the specified lighting conditions.Three different layer variations are being used here. Our layer dependence is determined by choosing a)2 layers of rGO, b)2 layers of rGO and 1 layer of GQD, c) 2 layers of rGO and 2 layers of GQD. Heterojunction between these two materials and their different dimensions enables the memory operation of the device.

- **Diffuse reflectance spectroscopy (DRS) of Devices :**

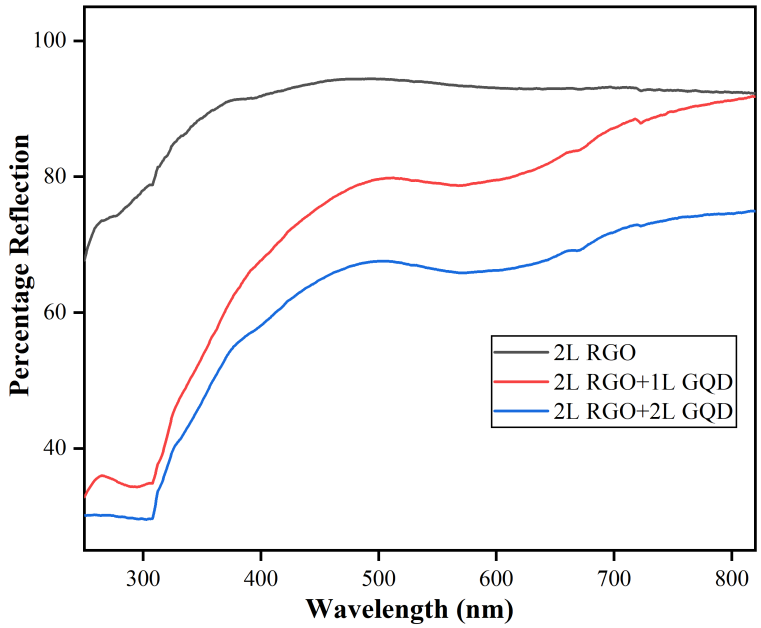
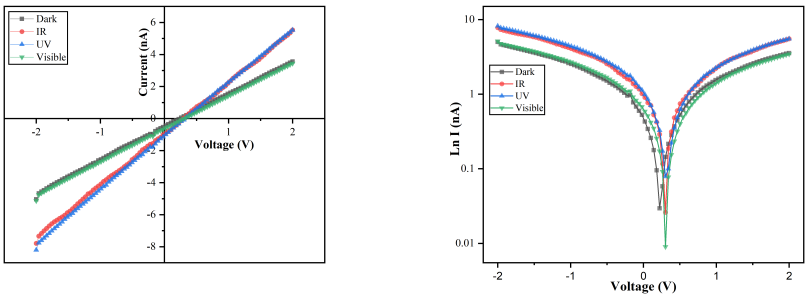
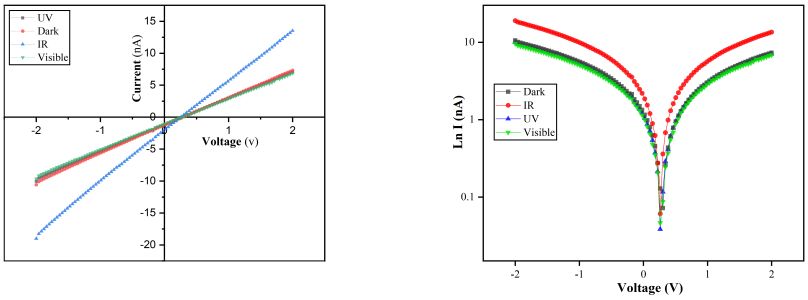


Figure 7.1: **DRS Plot of Devices with different layer numbers.**

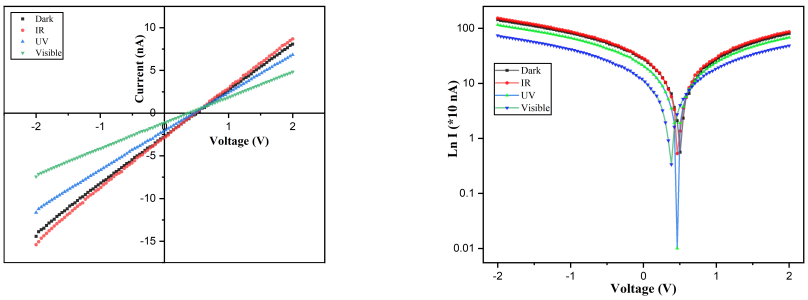
According to the results above, the device with two rGO layers exhibits 95% reflectivity, while the other two devices have substantially lower reflectance when compared to the first device. The devices with GQD layers exhibit a noticeable variation in reflectance between 500 and 800 nm. For our devices, near-IR to IR light (500-800 nm) will therefore be optimally absorbed.



(a) 2 Layers of rGO



(b) 2 Layers of rGO and 1 Layers of GQD.



(c) 2 Layers of rGO and 2 Layers of GQD.

Figure 7.2: **I-V characteristic and LogI-V Plot of different layered devices.**

- **Particularities and Conclusions from Fig. 7.2 Results :**

1. It is very obvious from the aforementioned I-V charts that the device is displaying appropriate current variations at (-ve) bias because of the presence of various lights illumination.

2. At -2 V our device is showing best response of change in current.

3. The asymmetry nature of last two logI-V plots confirms the hetero-junction formation between two materials.

4. One of the interesting fact of above I-V plot is it gives a (-ve) current at zero bias. The primary cause of this current is flowing of minority carriers which induces some diffusion current.

5. Finally, If we compare all the light illuminated current value then **IR shows best performance** out of all at -2 V which is also expected from the DRS results of device.

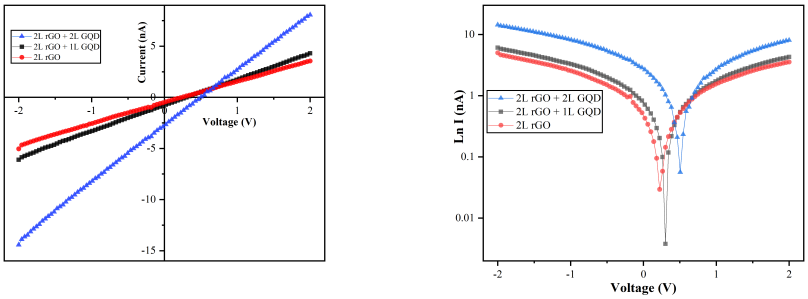
7.2 Device Performance with a specific Incident Light :

The performance of the devices is discussed in this section in a specific context.IR provides the best response when compared to other light illuminations, as we evaluated in the preceding section.We can therefore determine which device with a certain layer number and variation is the best based on the results of this section.

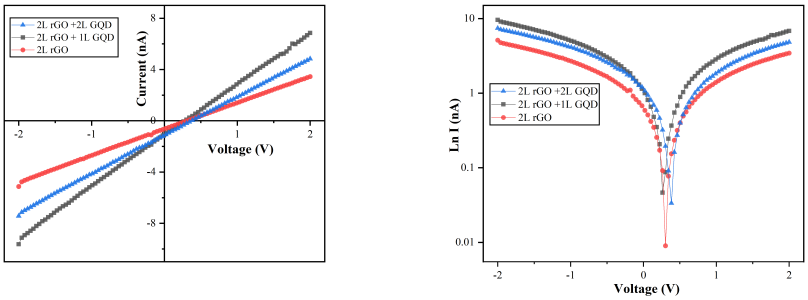
- **Particularities and Conclusions from Fig. 7.3 Results :**

1. If we compare the above results, then it seems very clustered but we should only focus on IR irradiation as we get the best response from this.

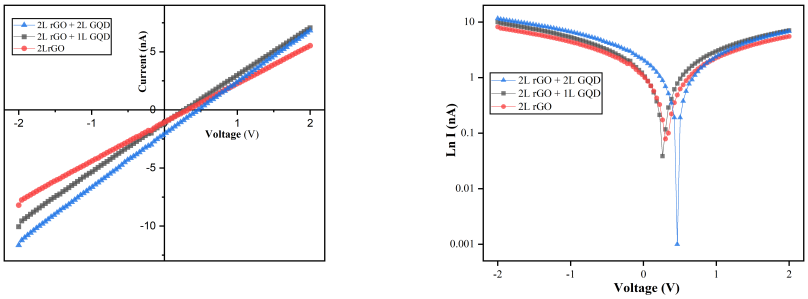
2. If we carefully see the results of I-V of IR radiated device then 2 layered rGO and 1 Layered GQD provides best response.



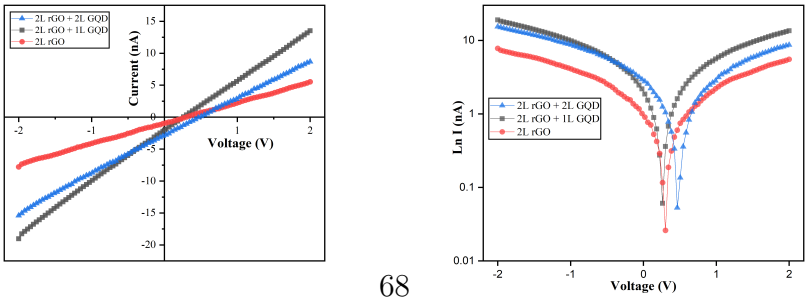
(a) Under Dark.



(b) Under Visible Light Illumination.



(c) Under UV Light Illumination.



(d) Under IR Light Illumination.

Figure 7.3: **I-V characteristic and LogI-V Plot under different light illumination.**

3. Our experimental data could have the following possible explanations: a) A greater number of layers results in a much larger depletion region between the two materials, which reduces the attenuation depth of the absorbed photons. As a result, there are fewer electron-hole pairs created, which leads to extremely little flow of current. That's why 2 layered rGO and 2 layered GQD device isn't showing proper response.

   b) The transmission of holes or electrons to the depletion zone will take significantly longer due to the rise in layer number. Now if there is any defect or any holes/electrons in that region already, then the recombination rate will become higher than the drift mechanism of the majority carriers.

7.3 Optimization of Device :

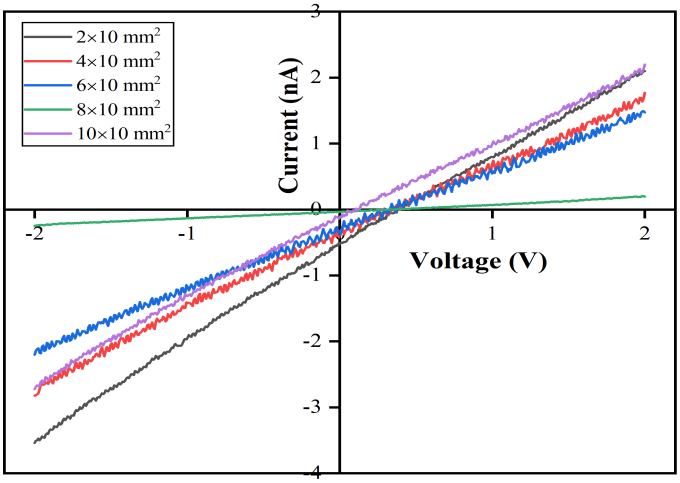
Now. we optimize the exposed surface are better to say channel region to get the proper responsivity and detectivity. The procedure to get the optimized device we already discussed that in chapter 6.

- **Particularities and Conclusions from Fig. 7.4 Results :**

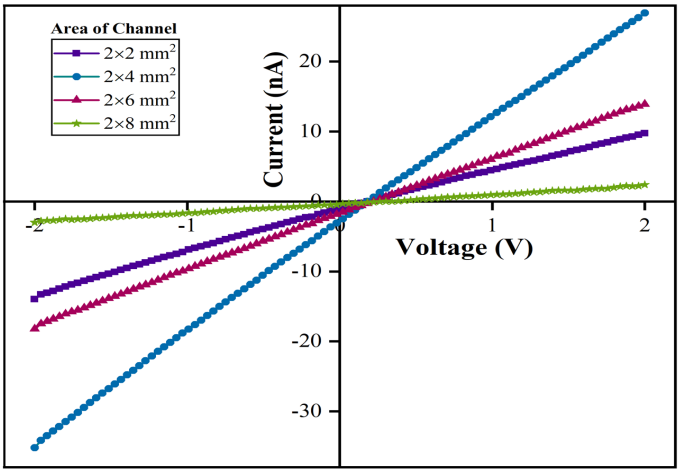
1. Out of all the devices evaluated, the one with a 2×10 mm^2 channel region has the best response, as shown in Fig. 7.4 (a).

2. If we examine the responses of the breadth-wise devices performance, the device with the highest performance is the 2×4 mm^2 areal surface, as shown in Fig. 7.4 (b).

3. From the above mentioned results it is pretty clear as the exposed surface area reduced, the current response getting better. One of the reason is that due to the less surface area the scattering of the electron-hole pairs will get reduce.



(a)



(b)

Figure 7.4: **(a) Length-wise and (b) Breadth-wise Optimization of device.**

7.4 Selection of proper Intensity of Light :

In this section we would discuss about the variation of current with different powered incident light. Later on depending upon the results, we will check the Responsivity (R) of our device for each intensity of light which will help us to find out proper intensity of light. Responsivity (R) in the reverse bias is calculated using $R = \frac{I_p - I_d}{P_{in}}$ formula, where I_p, I_d, P_{in} are the photo-current, dark current and incident power of light. From the results and calculations

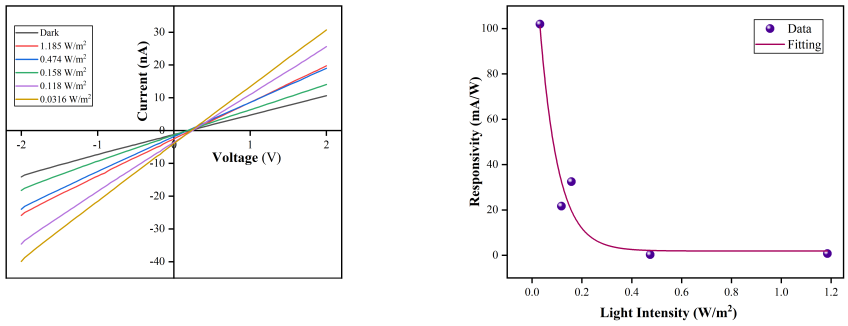


Figure 7.5: **(Left to Right) Variation of Photo-current with different Intensity of Light, Resonsivity with different light intensity.**

of responsivity, light having 31.6 mW/m^2 posses best responsivity compared to all.

Finally we go further with the memory operation of the device having **a) 2 Layers of rGo and 1 Layer of GQD** under **IR light** illumination posses **c) 31.4 mW/m^2 intensity** with channel region **c) 2×4 mm^2.**

7.5 Evaluating the performance of Memory function :

7.5.1 Excitory Post Synaptic Current (EPSC)Variation:

The Excitory Post Synaptic Current (EPSC) response had been investigated for rGO/GQD heterostructure based photo-synapse as a function of IR light

spike. The EPSC of biological synapse can be varied according to the duration of the light spike.

First, we study the performance of EPSC with the operating voltage -2 V and -1 V respectively [Fig.7.6], where -2 V gives better retention time compared to -1 V operating voltage under a light spike of time duration 5 sec.So, to check the memory operation we fixed the operating voltyage at -2 V.

Fig. 7.7 displays the variation of EPSC with our synaptic device under a series of different pulse duration light spikes which varies from 2 sec to 10 sec between a pulse interval of 2 sec. After the light pulse ended, the EPSC rapidly rose to its maximum value and then progressively dropped to a low current condition as the light was turned off. This kind of EPSC is the basis of realizing the computational function for human brain. When the active layer was activated by an optical signal, there was typically a fast spike in photo-generated carriers, which led to a sharp increase in EPSC. Slow current decay indicates in reduced photo carrier decay, closely resembling how the human brain stores memories.

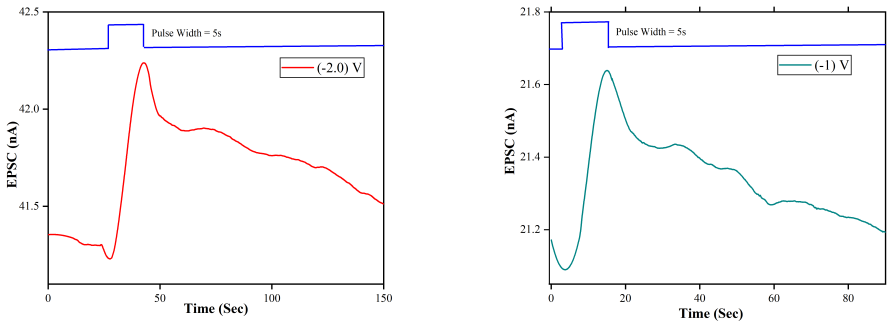


Figure 7.6: **(Left to Right) EPSC at operating voltage -2 V and -1 V .**

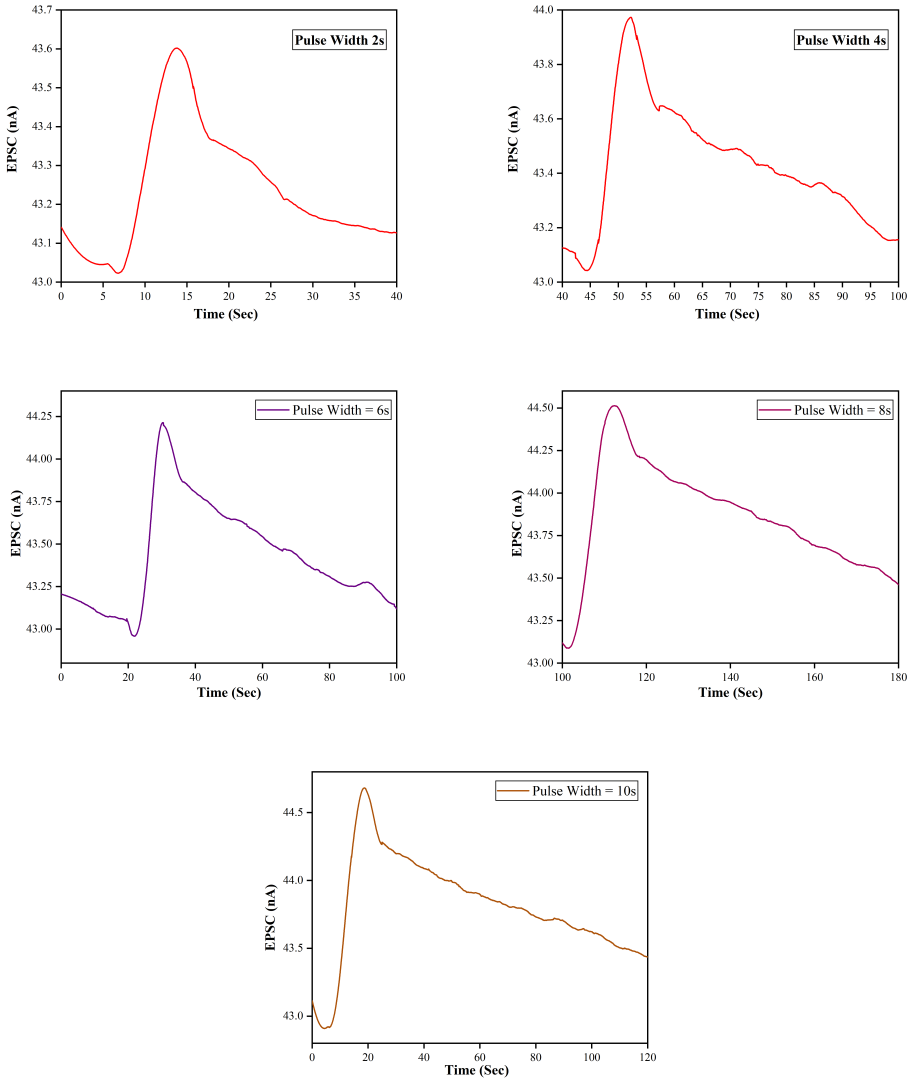


Figure 7.7: **EPSC evoked by different light pulse width.**

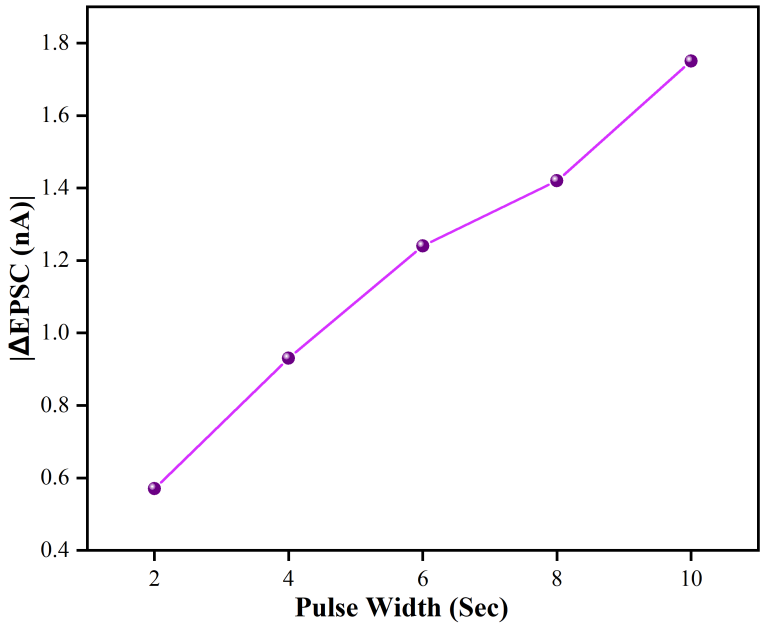


Figure 7.8: **Variation of EPSC with pulse width under a light pulse.**

The current change value, or ΔEPSC, is computed by deducting the initial dark current from the current during a light pulse. Keep in mind that a longer pulse duration can result in a higher ΔEPSC. As the pulse duration increases the photo-generated carriers becomes higher which results higher Δ EPSC.

7.5.2 Pair Pulse Facilitation (PPF) Index :

PPF index is a synaptic process where synaptic responses can be enhanced due to the stimulation of two successive presynaptic pulses. This is connected to the recognition and decoding of temporal information of visual signals and is another characteristic manifestation of Short Term Plasticity (STP) in a biological synapse.

The PPF like behavior has been shown in Fig. 7.9 of our device with pulse width of 2 sec and a pulse difference of 6 sec. Figure 7.9 shows that

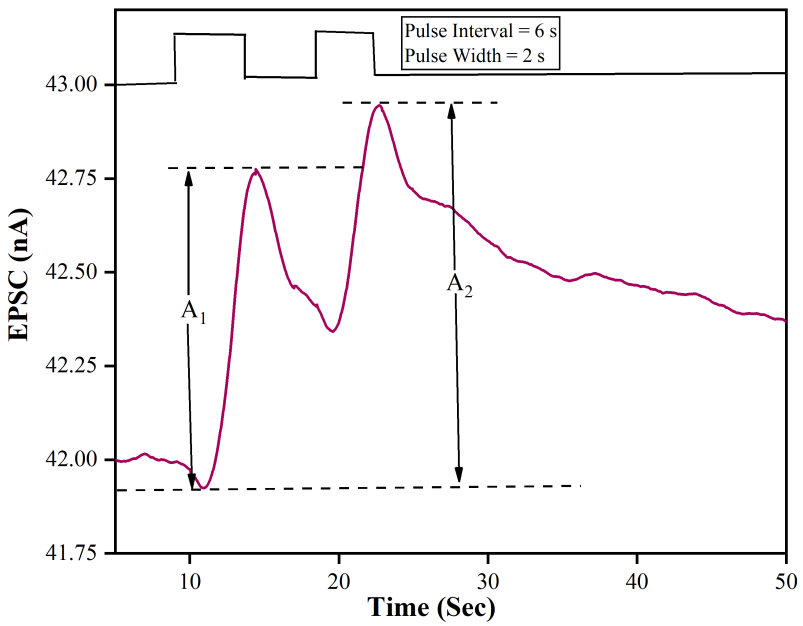


Figure 7.9: **EPSC triggered with two successive pulses**

the second photoresponsive current value (A2) is obviously higher than that induced by the first light pulse (A1). When the first light pulse was applied to the synaptic device, the photoinduced electrons and holes were generated in the rGO/GQD film, resulting in the increase of EPSC. The photogenerated electrons and holes were unable to fully recombine when the initial pulse was removed due to the large energy barrier between the two materials, which results in increased amplitude . PPF Index can be calculated with follwing formula;

$$\begin{aligned} PPF &= \frac{A_2}{A_1} \times 100\% \\ or &= \frac{A_2 - A_1}{A_1} \times 100\% \end{aligned}$$

where A2 and A1 are the values of the first and the second photoresponsive current, respectively.

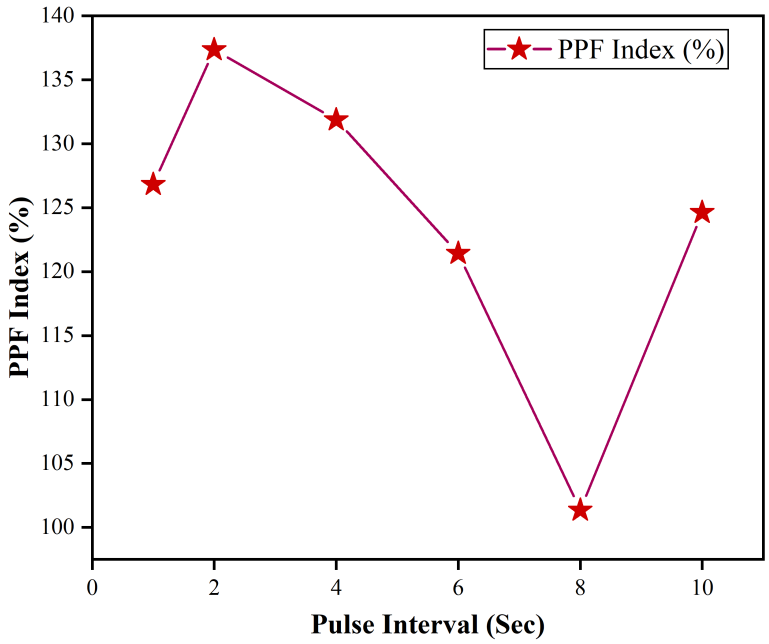
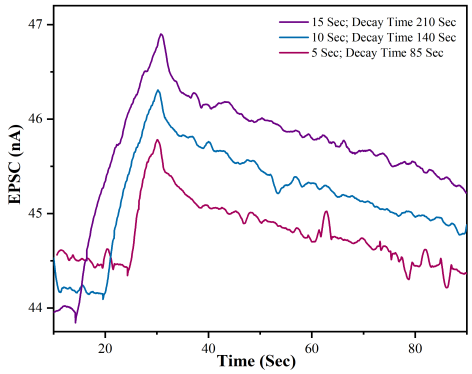


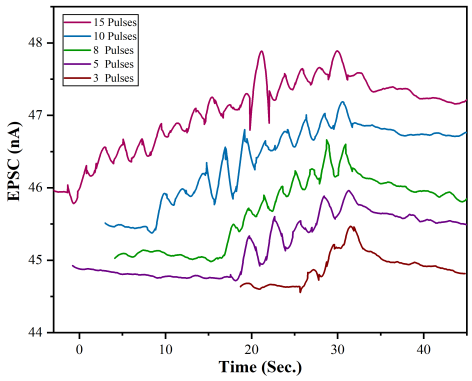
Figure 7.10: **Variation of PPF index with pulse interval between two light pulses.**

7.5.3 Plasticity Performance (Transition from STM to LTM) :

LTP corresponding to Long Term Memory (LTM) is another example of synaptic plasticity and is thought to be the basis for brain function. LTM is typically predicated on the synapses' by STM to LTM transition, which can be accomplished by both lengthening the pulse width and repeating rehearsal events. Here, by varying the quantity and width of the pulsed light stimuli, we were able to replicate the synaptic transition process for the rGO/GQD based PST for STM to LTM conversion.



(a)



(b)

Figure 7.11: **Left to Right) Transition from STP to LTP by increasing pulse width and pulse number.**

As shown in the Fig. 7.11 with the increase of light stimulas' width and light pulse number from 5sec to 15 sec and 3 pulses to 15 pulses respectively, the EPSC of the device increased remarkably and a longer decay time was needed to return into the original initial state after the removal of light spikes which indicated the transition from LTM to STM. In order to examine the memory ability of the device after provoking the relative EPSC intensity was determined using the formula I/I_0, where I represents the EPSC at a particular timepoint and I_0 denotes the starting current.

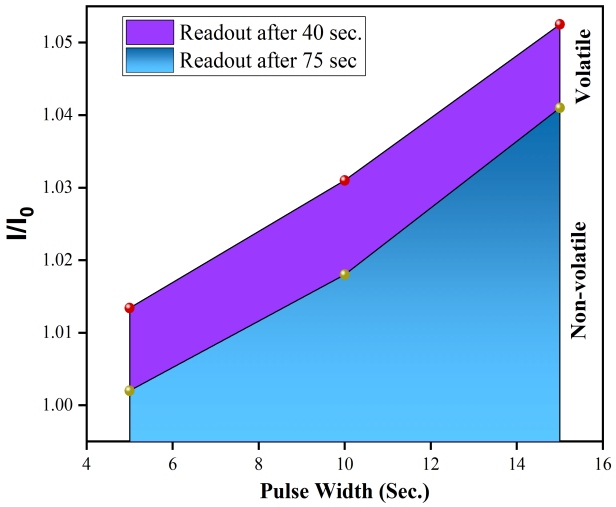


Figure 7.12: **Relative Intensity changes of EPSC with light pulse width.**

Following the removal of light pulses for 40 and 75 seconds, Figure 7.12 displays the relative intensity of EPSC; the purple and blue regions represent the volatile and nonvolatile portions, respectively. The blue zone, which can be improved as a function of light impulse width, is where the long-term memory was found. The human brain's memory rule is consistent with this fading memory tendency.

Bibliography

[1] "Perovskite/Organic Semiconductor-Based Photonic Synaptic Transistor for Artificial Visual System" Dandan Hao, Junyao Zhang, Shilei Dai, Jianhua Zhang, and Jia Huang; ACS Appl. Mater. Interfaces 2020

[2] "Photonic synaptic transistors with new electron trapping layer for high performance and ultra-low power consumption" Taewoo Kim and Kwang-Seok Yun ; www.nature.com/scientificreports

[3] "Retina-Inspired Carbon Nitride-Based Photonic Synapses for Selective Detection of UV Light"; Hea-Lim Park, Haeju Kim, Donggyu Lim, Huanyu Zhou, Young-Hoon Kim,Yeongjun Lee, Sungjin Park, and Tae-Woo Lee; Advanced Materials; https://doi.org/10.1002/adma.201906899

[4] "A Photoelectric-Stimulated MoS2 Transistor for Neuromorphic Engineering"; Shuiyuan Wang, Xiang Hou, Lan Liu, Jingyu Li, Yuwei Shan, Shiwei Wu, David Wei Zhang, and Peng Zhou; AAAS Research Volume 2019, Article ID 1618798, 10 pages https://doi.org/10.34133/2019/1618798

[5] "Recent Progress in Photonic Synapses for Neuromorphic Systems"; Junyao Zhang, Shilei Dai, Yiwei Zhao, Jianhua Zhang, Jia Huang; https://doi.org/10.1002/aisy.201900136

Chapter 8

Conclusion and Future Work :

- **Conclusion :**

In summary, we used a straightforward hydrothermal technique to synthesis both rGO and GQD in a single step. Following material preparation, spin coating was utilized to build the photonic synapse. We just used I-V characteristics to look at the materials' ideal layer numbers. Following layer number tuning, we assess the precise level of light exposure under which our device demonstrated flawless memory functions. After that, we began to shrink the device's channel region, which was subsequently examined once more using the I-V curve. Finally, we adjusted the light's intensity such that it would be ideal for examining synaptic behaviour.

Finally we were able to contract a photo-synapse based on the heterostructure of **2 layers of rGO** and **1 layer of GQD** which is showing very good synaptic behaviour under **low intensity (0.0316 W/m^2)** of **IR illumination** with a channel region of **2×4 mm^2**. Due to the good photosensitivity of GQD and excellent charge mobility performance of rGO our device is showing tremendous synaptic performance even in the very low intensity of light. Fundamental synaptic performance like ΔEPSC, PPF, Plasticity i.e. transition from STM to LTM with method of approaches have been successfully stimulated.

- **Future Work :**

1. Photonic Synaptic Transistor is now one of the emerging device in the field neuromorphic computing. Using GQDs as it's photo-sensitive

layer would be a very beneficial point for it's large surface area, size tunability etc. It's heterojunction with rGO or any other 2D transitional materials will definitely increase the performance of memory operation.

2. The key point of our device it shows the synaptic behaviour in a very low light intensity of IR. Due to this low power consumption the thermal noise isn't showing much effectiveness in our case which is one of the big issue while working with IR.

3. Our future plan is to integrate our device with some Artificial Intelligence (AI) model that will be programmed as of Image recognition.

4. By associating our device we can also able to make night vision sensor and choosing a flexible substance enhance the durability of the device.

5. It is conceivable to store a very large number of bits if our device can be manufactured as an array. We can even create a smaller version of the GPU by figuring out the array's weight function and creating the necessary code.